

Accurate Predictions of Volatile Plutonium Thermodynamic Properties

Sophie Kervazo,¹ Florent Réal,¹ François Virot,² André Severo Pereira Gomes,¹ and Valérie Vallet¹

¹*Univ. Lille, CNRS, UMR 8523 - PhLAM - Physique des Lasers Atomes et Molécules, F-59000 Lille, France**

²*Institut de Radioprotection et de Sécurité Nucléaire (IRSN) PSN-RES, Cadarache, Saint Paul Lez Durance 13115, France*

The ability to predict the nature and amounts of plutonium emissions in industrial accidents, such as in solvent fires at PUREX nuclear reprocessing facilities, is a key concern of nuclear safety agencies. In accident conditions and in the presence of oxygen and water vapor, plutonium is expected to form the three major volatile species PuO_2 , PuO_3 , and $\text{PuO}_2(\text{OH})_2$, for which the thermodynamic data necessary for predictions (enthalpies of formation and heat capacities) presently show either large uncertainties or are lacking. In this work we aim to alleviate such shortcomings by obtaining the aforementioned data via relativistic correlated electronic structure calculations employing the multi-state complete active space with second-order perturbation theory (MS-CASPT2) with state-interaction RASSI spin-orbit coupling approach, which is able to describe the multireference character of the ground-state wave functions of PuO_3 and $\text{PuO}_2(\text{OH})_2$. We benchmark this approach by comparing it to relativistic coupled cluster calculations for the ground, ionized, and excited states of PuO_2 . Our results allow us to predict enthalpies of formation $\Delta_f H^\circ(298.15\text{ K})$ of PuO_2 , PuO_3 , and $\text{PuO}_2(\text{OH})_2$ to be -449.5 ± 8.8 , -553.2 ± 27.5 , and $(-1012.6 \pm 38.1)\text{ kJ mol}^{-1}$, respectively, which confirm the predominance of plutonium dioxide, but also reveal the existence of plutonium trioxide in the gaseous phase under oxidative conditions, though the partial pressures of PuO_3 and $\text{PuO}_2(\text{OH})_2$ are nonetheless always rather low under a wet atmosphere. Our calculations also permit us to reassess prior results for PuO_2 , establishing that the ground state of the PuO_2 molecule is mainly of $^5\Sigma_g^+$ character, as well as to confirm the experimental value for the adiabatic ionization energy of PuO_2 .

INTRODUCTION

A key step in the reprocessing of spent nuclear fuel is the PUREX (plutonium uranium refining by extraction) liquid-liquid process, through which uranium and plutonium are separated from the minor actinides. Thanks to its remarkable selectivity and the stability properties, tri-n-butyl phosphate (TBP) is used as the organic extractant. However, its high viscosity and density impose that the organic phase should be diluted within a hydrocarbon solvent. In the French La Hague reprocessing plant, hydrogenated tetrapropylene (HTP) is currently used as a TBP diluent. As HTP is a highly flammable substance, this could, in case of an accidental event, trigger a fire of the uranium-plutonium containing organic solvent and may thus induce a release in the environment and atmosphere of highly radioactive species. The knowledge of their chemical behaviors is thus mandatory to carry out safety and risk analysis.

The presence of plutonium induces considerable difficulties to perform experimental investigations of solvent fires. One way to overcome these is to use a plutonium surrogate in order to carry out fire experimental campaigns. To make a selection of surrogate candidates, their behavior should be similar in all oxidation states. Considering for example the gaseous state, the volatility of Pu(VI) , which still remains an open issue, should be addressed specifically because some of the candidates (Th, Ce) [1] cannot extend their oxidation degree up to VI. An alternative to surrogates is the development of a predictive model which includes all relevant physical and

chemical transformations of plutonium-containing substances. Whatever the case, both approaches need reliable and accurate molecular properties of the gaseous species involved in the $\text{Pu}+\text{O}+\text{H}$ system, required to calculate their thermodynamic properties.

The thermodynamic properties of the $\text{Pu}+\text{O}+\text{H}$ system have been widely studied and assessed (see refs 2 and 3] and the references therein). Nonetheless, some uncertainties remain in the thermodynamic properties of some species: for the gaseous plutonium dioxide, PuO_2 , the assessment of its standard heat of formation reveals a discordance between second and third law analyses of experimental data [2]. In addition, experimental data (and in particular thermodynamic data) for other Pu(VI) molecules, such as $\text{PuO}_2(\text{OH})_2$ and PuO_3 , are scarce, and their existence in the gaseous phase remains an open question. Ronchi et al. [4] have carried out mass spectrometric measurements of effusing vapor over plutonium oxide sample where $\text{PuO}_3(\text{g})$ has been detected but only as a nonequilibrium species. Then, transpiration experiments of plutonium oxide have been performed by Krikorian et al. [5] under oxygen as well as a mixture of oxygen and steam. From analogies with gaseous uranium species, the authors considered $\text{PuO}_2(\text{OH})_2$ and PuO_3 molecules as the effusing species. Hübener et al. [6] have studied by thermochromatography the volatility of plutonium oxide under wet oxygen flux, and their results highlighted the formation of volatile Pu(VI) expected as $\text{PuO}_2(\text{OH})_2$.

To predict the respective quantities of the three target volatile products of plutonium in the presence of oxygen or steam, accurate thermal functions (heat capacity,

entropy, enthalpy increment) and enthalpies of formation are needed. For gas-phase molecules, this all boils down to having data on their electronic structure in order to directly calculate the vibrational-rotational partition functions. The electronic partition functions in turn require the knowledge of all the low-lying excited states within $10\,000\text{ cm}^{-1}$ and their spectroscopic labeling as degeneracies enter the statistical weights. If not known from direct spectroscopic measurements, these are often roughly estimated from chemically and spectroscopically analogous systems, such as crystals or molecules containing another actinide. However, the investigation of plutonium-containing molecules with quantum chemical methods remains a big challenge because they exhibit complex electronic structures, and as such it is often of little use to estimate their properties from chemical analogues. The presence of open 5f, 6d, and 7s orbitals on the plutonium atom leads to dense valence electronic spectra, in which the numerous degenerate or quasi-degenerate electronic states are suspected to have strong multireference characters.

A potential route for handling electron correlation and relativistic effects simultaneously for multireference heavy element complexes is to work in the four-component (4C) framework, with the Dirac-Coulomb, Dirac-Coulomb-Gaunt, or Dirac-Coulomb-Breit Hamiltonian or with the exact two-component (X2C) approaches using a molecular mean-field (MMF) approach [7] (${}^2\text{DC}^{\text{M}}$). The multireference intermediate Hamiltonian Fock-space coupled cluster (IHFSCC) has been successfully applied to actinide-containing molecules [8, 9], though with available implementations it is not possible to treat states differing by more than two electrons from a closed-shell reference. This is problematic for PuO_3 , which turns out to have a complex multireference ground-state with significant contributions from configurations with two or even four unpaired electrons [10–18]. On the other hand, at the fully relativistic level, PuO_2 turns out to have a closed-shell ground state, allowing us to also estimate its standard enthalpy of formation with coupled-cluster single and double with perturbative triples (${}^2\text{DC}^{\text{M}}\text{-CCSD(T)}$) calculations. The recent implementation of the fully relativistic EOM-CCSD method [19] offers the possibility to accurately compute the ionization potential (IP) of the PuO_2 molecule, and new arguments are proposed to clarify why the experimental values reported by Rauh et al. [20, 21] and Capone et al. [22] differ by about 3 eV from the IP value measured by Santos et al. [23].

Considering ${}^2\text{DC}^{\text{M}}\text{-CCSD(T)}$ to be the gold standard – it was shown by Shee et al. [19] that ${}^2\text{DC}^{\text{M}}$ Hamiltonian yields results which are nearly indistinguishable from the Dirac-Coulomb Hamiltonian – and the fact that there are more experimental data estimating the enthalpy of formation, the PuO_2 molecular system represents an excellent candidate to benchmark relativistic multiref-

erence methods with an *a posteriori* treatment of the spin-orbit coupling (SOC) interaction, namely the state-interaction-multistate second-order perturbation theory RASSI-MS-CASPT2 approach, hereafter referred to as SO-CASPT2, which has been used to compute the thermodynamic data of PuO_3 and $\text{PuO}_2(\text{OH})_2$. High accuracy is achieved by extrapolating the electronic energies to the complete basis set limit.

The details of the calculations are described in the following section, followed by a discussion of the electronic structure of the three aforementioned molecules. We continue with an analysis of the thermodynamic properties and a comparison to available experimental data and propose new heat capacity functions and standard entropies and enthalpies of formation. Finally, the volatility of Pu(VI) species is investigated within the framework of thermodynamic equilibrium calculations. The article closes with conclusions and perspectives for nuclear safety related issues.

COMPUTATIONAL DETAILS

Chemical Reactions Used to Derive the Standard Enthalpies of Formation of PuX Molecules

To determine the enthalpies of formation, $\Delta_{\text{f}}H^{\circ}(298.15\text{ K})$, of the different plutonium oxides and oxyhydroxides, we consider the reactions presented in Table I. We begin by computing the enthalpies of the reactions presented in Table I, as:

$$\Delta_{\text{r}}H^{\circ} = \sum_i (E_i + ZPE_i + [H^{\circ}(298.15\text{ K}) - H^{\circ}(0\text{ K})]_i), \quad (1)$$

that is by summing up electronic energies E_i , the vibrational zero point energies (ZPE_i) and the enthalpy increment, $[H^{\circ}(298.15\text{ K}) - H^{\circ}(0\text{ K})]_i$ at 298.15 K (see Table S1) for the products, minus that of the reactants. For a generic reaction leading to the formation of PuX ($\text{Pu} + \text{A} \longrightarrow \text{PuX} + \text{B}$), the standard enthalpy of formation, $\Delta_{\text{f}}H^{\circ}(298.15\text{ K})$, is computed as

$$\Delta_{\text{f}}H^{\circ}(\text{PuX}) = \Delta_{\text{r}}H^{\circ} - \Delta_{\text{f}}H^{\circ}(\text{B}) \quad (2)$$

$$+ \Delta_{\text{f}}H^{\circ}(\text{Pu}) + \Delta_{\text{f}}H^{\circ}(\text{A}), \quad (3)$$

using the known enthalpies of formations of the Pu and A reactants and the B product listed with their uncertainties in Table S1 in the Supporting Information [24, 25]. Note that, because of the lack of thermodynamics data on plutonium species, it is not possible to use reactions that are isogyric or isodesmic, which might alter the final accuracy of our results; the measure of the resulting uncertainties within the 95% confidence limit obtained for the average of these reactions is computed as explained in the Supporting Information, and reported in Table IX.

TABLE I: Reactions Used to Derive the Standard Enthalpies of Formation of PuO₂, PuO₃, and PuO₂(OH)₂

	PuO ₂	PuO ₃	PuO ₂ (OH) ₂
R ₁	Pu + O ₂ → PuO ₂	Pu + $\frac{3}{2}$ O ₂ → PuO ₃	Pu + O ₂ + 2 H ₂ → PuO ₂ (OH) ₂
R ₂	Pu + 2 O → PuO ₂	Pu + 3 O → PuO ₃	Pu + 4 O + 2 H → PuO ₂ (OH) ₂
R ₃	Pu + H ₂ O ₂ → PuO ₂ + H ₂	Pu + $\frac{3}{2}$ H ₂ O ₂ → PuO ₃ + $\frac{3}{2}$ H ₂ O	Pu + 3 H ₂ O ₂ → PuO ₂ (OH) ₂ + 2 H ₂ O
R ₄	Pu + 2 OH → PuO ₂ + 2 H	Pu + 3 OH → PuO ₃ + 3 H	Pu + 4 OH → PuO ₂ (OH) ₂ + 2 H
R ₅	Pu + 2 H ₂ O → PuO ₂ + 2 H ₂	Pu + 3 H ₂ O → PuO ₃ + 3 H ₂	Pu + 4 H ₂ O → PuO ₂ (OH) ₂ + 2 H ₂
R ₆	Pu + 2 H ₂ O → PuO ₂ + 4 H	Pu + 3 H ₂ O → PuO ₃ + 6 H	Pu + 4 H ₂ O → PuO ₂ (OH) ₂ + 6 H

Two-Step Relativistic Calculations

Geometries and Enthalpy Corrections

The geometries were obtained from scalar relativistic DFT calculations, except for PuO₂, for which the optimal ²DC^M-CCSD(T) geometry was used. In the DFT calculations, the plutonium atom was described by a relativistic effective core potential (RECP) ECP60MWB [26] with the corresponding basis set of quadruple- ζ quality [27], while for the lighter atoms augmented triple ζ (aug-cc-pVTZ) [28] basis sets were used. All of the DFT calculations were carried out with the B3LYP functional [29] and the GAUSSIAN09 [30] package. The ZPE values and enthalpy corrections needed in eq. 1 were calculated from the harmonic vibrational frequencies. Anharmonic corrections to the vibrational partition functions were not included, as these would contribute only a few tenths of a kJ mol⁻¹ at most and only for those species involving hydrogen atoms. Using the vibrational perturbation theory [31, 32] as implemented in Gaussian [30], we have computed the anharmonic corrections for all molecules. The largest contribution to any of the reaction enthalpies was only 5 kJ mol⁻¹, even at temperatures as high as 3000 K, which is considered negligible for the accuracy goal of the present work.

Basis Sets and Extrapolation to the Complete Basis Set Limit

To reach high accuracy for *ab initio* thermochemistry, the computed electronic energies were extrapolated to the complete basis set limit (CBS), from two calculations with all-electron atomic natural orbitals relativistic core correlation (ANO-RCC) basis sets [33, 34] with quality sequentially increased from triple- ζ (n=3) to quadruple- ζ (n=4). The CASSCF/HF energies were extrapolated with the Karton and Martin formula [35]:

$$E_n^{\text{CAS}/\text{HF}} = E_{\text{CBS}}^{\text{CAS}/\text{HF}} + A(n+1) \exp(-6.57\sqrt{n}), \quad (4)$$

separately from the correlation energies E_n^{corr} via [36, 37]

$$E_n^{\text{corr}} = E_{\text{CBS}}^{\text{corr}} + \frac{B}{(n+1/2)^4}. \quad (5)$$

While irregular basis convergence patterns was reported for lanthanide ANO-RCC basis sets [38], the convergence

is smooth in the case of the Pu basis sets as illustrated by Figure S1 in the Supporting Information.

Single Reference Wave Function Correlated Calculations

To account for dynamic electronic correlation, in cases of open-shell systems with a weak multireference character, UCCSD(T) (unrestricted coupled cluster singles doubles and perturbative triples) [39] is the gold standard. These calculations were performed using the Molpro Quantum Chemistry software [40]. The frozen orbitals were the 1s orbital of O and 1s to 5d (included) orbitals of Pu. Core-valence correlation effects were discarded not only due to their high computational cost but also because we expect them to be no larger than 4 kJ mol⁻¹ for actinide molecules [41, 42]. Due to the important multiconfigurational character of the ground-state wave function of PuO₃ and PuO₂(OH)₂ species, no UCCSD(T) calculations were performed.

Multireference Calculations and Definition of the Orbital Active Spaces

Knowing the multi-configurational character of the ground-state wave function of the atomic plutonium and the plutonium oxides and oxyhydroxides of interest [10], and since SOC needs to be included *a posteriori* [43], the use of a multi-configurational approach that accounts for the static and dynamic electronic correlation effects is mandatory. The former was included with the CASSCF (Complete Active Space Self Consistent Field) method [44, 45]. The active spaces are listed in the Table II; for the atoms (O, H, Pu) and molecules without Pu (OH, H₂O₂, H₂, H₂O), the active space is composed of the valence orbitals. Nevertheless, one has to note that the CAS (Complete Active Space) of (8,13) for the plutonium atom lead to convergence problems as the competing configurations 5f⁶7s², 5f⁶6d¹7s¹, 5f⁶6d¹7s²7p¹ are close in energy and intertwined. [46–48] We instead used a RAS (Restricted Active Space) [49] to focus on the two configurations 5f⁶7s², 5f⁶6d¹7s¹ that dominate the low-lying part of the Pu spectrum (up to 18 000 cm⁻¹). The RAS space includes the 7s in the RAS1, the 5f in the RAS2 and the 6d in RAS3 with one as the maximum number of holes in RAS1 and as number of particles in RAS3.

TABLE II: Active Spaces for the Various Plutonium Oxides and Oxyhydroxides

molecule	active space (electron, orbitals)	orbitals
PuO ₂	(4,4) ^a	$\delta_u(2), \phi_u(2)$
PuO ₂	(12,17) ^b	$\pi_u(2), \pi_g(2), \sigma_g, \sigma_u, \pi_u^*(2), \pi_g^*(2), \sigma_g^*, \sigma_u^*, \delta_u(2), \phi_u(2), \delta_g(2)$
PuO ₃	(14,13) ^c	$1a_1, 2a_1/\pi_u, 2a_1, 4a_1/p_x^o, 5a_1/\phi_u,$ $6a_1/\pi_u, 1b_1/\phi_u, 2b_1/\pi_u, 1b_2/p_z^o, 2b_2/\sigma_u, 3b_2/\delta_u, 4b_2/\sigma_u^*, 1a_2/\delta_u$
PuO ₂ (OH) ₂	(4,4)	$1a/\delta, 2a/\phi, 1b/\delta, 2b/\phi$
Pu	(8,13)	7s, 5f, 6d
O	(6,4)	2s, 2p _x , 2p _y , 2p _z
O ₂	(12, 8)	$\sigma_{2s}, \sigma_{2s}^*, \sigma_{2p}, \sigma_{2p}^*, \pi_{2p}(2), \pi_{2p}^*(2)$
OH	(7,5)	$\sigma, \sigma_{nb}, 2p_x^o, 2p_y^o, \sigma^*$
H ₂ O ₂	(14, 10)	$1 \sigma^{O-O}, 1 \sigma^{*O-O}, \sigma^{O-H}(2),$ $2 \sigma^{O-O}, \pi^{O-O}, 2p^o, 1 \sigma^{*O-O}, \sigma^{O-H}(2)$
H ₂ O	(8,6)	$2a_1, 1b_2, 3a_1, 1b_1, 4a_1, 1b_2$
H ₂	(2, 2)	σ_g, σ_u^*
H	(1,1)	1s

energy calculation.

^b For ground and excited-states that are coupled by the spin-orbit Hamiltonian in the RASSI.^c The orbital numbering refers to the active space, e.g. 1a₁ is the first active orbital of a₁ symmetry.

For the plutonium molecules, the difficulty is to design orbital active spaces that do not exceed the current active space limit of about 16 electrons in 16 orbitals. In a recent work, some of us have used the multireference density matrix renormalization group (DMRG) calculations [10], in which we could afford including all the valence orbitals from both Pu and oxygen atoms into the active space, thus allowing the maximum flexibility into the ground-state wave functions. These DMRG calculations cannot be used for quantitative thermodynamics calculations, as they were restricted to a DMRG-CI approach, and did not include orbital relaxation, dynamic correlation and SOC. However, concepts of quantum information theory, such as orbital-pair correlations, were helpful to identify which orbitals contribute most to the ground-state wave functions, helping the design of reduced “optimal” active spaces [10] that can be reasonably handled in the SO-CASPT2 calculations carried out here.

Regarding PuO₂ (symmetry D_{2h}), the choice of the active space to describe the low lying excited states was based on the work of Denning et al. [50] and La Macchia et al. [51]. The full valence active space is composed of 2 π_u , 2 π_g , σ_g , and σ_u bonding orbitals, which are combinations of 5f and 6d orbitals of plutonium mixed with the 2p orbitals of the oxygen atoms, the corresponding antibonding orbitals, and the four nonbonding δ_u , ϕ_u .

Despite the increase of the computational power, a CASSCF calculation with the full valence active space [10] made of 16 electrons in 19 orbitals is still not feasible (203 440 360 CSF for the $^5\Sigma_g^+$ ground state). We thus chose to remove two lowest doubly occupied π_g orbitals, leading to an active space of 12 electrons in 17 orbitals. Note that La Macchia et al. [51] used a smaller active space of 12 electrons in 14 orbitals, as they dis-

carded the π_g^* and σ_g^* antibonding orbitals. Whereas for a good estimate of SOC effect in a two-step approach, numerous excited states have to be computed (to position accurately the excited states with respect to the ground state), this could degrade the description of the ground state in terms of total energy and wave function [52]. Thus the ground-state $^5\Sigma_g^+$ spin-free energy is computed from the well-suited minimal active space that distributes four electrons in the four nonbonding orbitals (δ_u and ϕ_u), denoted SO-CASPT2(4,4).

To define the important orbitals in the active space of PuO₃ (symmetry C_{2v}), we used information from PuO₂²⁺ that can be considered as a subunit of plutonium trioxide suggesting an active space composed of two π orbitals, one σ orbital along with the corresponding antibonding associated to the plutonyl PuO₂²⁺ subunit, the four nonbonding δ_u and ϕ_u orbitals and the p_x, p_y and p_z of the third distant oxygen; this sums up to an active space of 14 electrons distributed in 13 orbitals as depicted in ref. 10. The active space to treat the cationic form PuO₃⁺ includes one electron less.

For PuO₂(OH)₂ (symmetry C_2), the strengths of the orbital-pair correlations depicted in ref. 10 indicate that the nonbonding δ_u and ϕ_u orbitals of Pu are the most entangled orbitals and should be part of a chemically relevant active space for the ground-state wave function as well as the low-lying excited states. This yielded 16 electronic excited spin-free states. For the other Pu systems, it was not possible to include all states. Indeed, the higher excited states turned out to have too low reference weights (<20%) in the Multi-State Complete Active Space with Second-Order Perturbation Theory (MS-CASPT2) [53] wave-functions.

The case of the Pu atom was peculiar since the RASSCF was not able to reproduce the exact degeneracy

of the states of the same L value. Therefore, the degeneracy was manually imposed across states with identical L and S values. The CASSCF and MS-CASPT2 calculations finally include 80, 119, and 16 electronic states for PuO_2 , PuO_3 , and $\text{PuO}_2(\text{OH})_2$, respectively as detailed in Table S6 in the Supporting Information. As for the UCCSD(T) calculations the 1s orbital of O and the 1s to 5d orbitals (included) for Pu were kept frozen. To guarantee a good description of all the states, an imaginary shift of 0.05 ua [54] was added to the zeroth-order Hamiltonian in addition to the IPEA = 0.25 ua correction [55].

Spin-Orbit Coupling State Interaction Method

For the Pu atom and the plutonium molecules, SOC was treated *a posteriori* by state interactions between the MS-CASPT2 wave functions, using the restricted active space state interaction (RASSI) program [56], with spin-orbit integrals computed in the atomic mean field approximation using the AMFI code [57, 58]. These results are referred to as SO-CASPT2. The SOC contributions to the ground-state energies, i.e. the difference between the ground-state spin-free MS-CASPT2 energies (SF-CASPT2) and the SO-CASPT2 energies, was added to all other scalar relativistic results, such as the DFT and UCCSD(T) results. In Table IX, ΔE_{SO} corresponds to the difference between the SOC contributions of the plutonium molecule and the atomic Pu. All SO-CASPT2 calculations were performed with the MOLCAS8 package [59].

One-step relativistic correlated calculations

We also performed one-step relativistic calculations based on the molecular mean-field [7] approximation to the Dirac-Coulomb (${}^2\text{DC}^{\text{M}}$) Hamiltonian, at MP2, CCSD and CCSD(T) [60, 61] levels of theory with DIRAC18 electronic structure code [62] for Pu, PuO_2 , H_2 , OH, H_2O and H_2O_2 . This allowed us to obtain the energies for reactions $\text{R}_3\text{--R}_6$ yielding PuO_2 .

The Dyll basis sets [63, 64] of triple- and quadruple-zeta quality were employed for the plutonium atom and Dunning aug-cc-pVnZ ($n = 3, 4$) sets [28] for the light elements, all of which are left uncontracted. These calculations have been performed in $D_{\infty h}$ symmetry for Pu, PuO_2 and H_2 , in $C_{\infty v}$ symmetry for OH, in C_{2v} symmetry for H_2O and in C_1 symmetry for H_2O_2 . In all cases, we've employed the approximation of the ($SS|SS$)-type two-electron integrals by a point-charge model [65]. Electrons in molecular spinors with energies between -3 and 100 ua were included in the correlated treatment, which amounted to correlating 28 electrons for PuO_2 , 16 for Pu, 12 for H_2O_2 , 6 for OH and H_2O , and 2 for H_2 .

For PuO_2 , the SCF calculations were closed-shell ones, with 52 and 58 electrons in g and u irreducible representations, respectively. For this species, the equilibrium structure and stretching frequencies were determined via a polynomial fit of the potential energy surface constructed from single-point calculations for symmetric and antisymmetric Pu-O stretching modes. Because of constraints in computational resources, the O-Pu-O bending mode frequency was obtained from ${}^2\text{DC}^{\text{M}}\text{-CCSD(T)}$ calculations correlating a smaller number of spinors between -3 and 5 ua. Energies and potential energy curves at the complete basis set limit were obtained with the same formula (Eqs. 4 and 5) introduced previously.

The Pu atom is converged at the Hartree-Fock level to the $J = 0$ ground-state, with 44 and 50 electrons in the g and u irreducible representations, respectively. For the hydroxy radical, the SCF calculation was performed using the average-of-configurations formalism [66], with 8 electrons taken as closed shell and 1 as open shell. In the open-shell coupled cluster model, the occupations of the different irreducible representations ($\Omega = 1/2, -1/2, 3/2, -3/2$) were restricted to be 3, 3, 1, 0, respectively. The internuclear distance used was that obtained at the DFT level (see section), as was the case for H_2 , H_2O , and H_2O_2 .

Apart from the ground-state MP2, CCSD, and CCSD(T) calculations, we performed equation-of-motion calculations for ionization potentials (EOM-IP-CCSD) for atomic Pu and PuO_2 , as well as excitation energies (EOM-EE-CCSD) [19] for PuO_2 , on the basis of the coupled cluster wave functions above.

In the case of EOM-IP-CCSD for Pu, we requested the number of states as follows: five $\Omega = 1/2_{\text{g}}$, two $\Omega = 3/2_{\text{g}}$, one $\Omega = 5/2_{\text{g}}$, three $\Omega = 1/2_{\text{u}}$, two $\Omega = 3/2_{\text{u}}$ and one $\Omega = 5/2_{\text{u}}$, whereas for PuO_2 we requested two $\Omega = 1/2_{\text{g}}$, one $\Omega = 3/2_{\text{g}}$, three $\Omega = 1/2_{\text{u}}$, two $\Omega = 3/2_{\text{u}}$ and one $\Omega = 5/2_{\text{u}}$ states. In the case of EOM-EE-CCSD we requested the number of states as follows: six $\Omega = 0_{\text{g}}$, four $\Omega = 1_{\text{g}}$, three $\Omega = 2_{\text{g}}$, two $\Omega = 3_{\text{g}}$, one $\Omega = 4_{\text{g}}$, one $\Omega = 5_{\text{g}}$, ten $\Omega = 0_{\text{u}}$, nine $\Omega = 1_{\text{u}}$, seven $\Omega = 2_{\text{u}}$, five $\Omega = 3_{\text{u}}$, three $\Omega = 4_{\text{u}}$, and one $\Omega = 5_{\text{u}}$.

RESULTS AND DISCUSSION

Electronic Structure Analysis

Atomic Pu

To compute the enthalpies of formation of the plutonium molecules, an accurate description of the plutonium atom, i.e. its electronic structure, is mandatory. Thus, in Table III and Table S2 in the Supporting Information, the SO-CASPT2 calculations are reported and compared to available data from the literature [46–48]. The SO-CASPT2 energy levels are able to accurately reproduce

TABLE III: Fine Structure Transition Energies (ΔE in cm^{-1}) of Atomic Pu Computed at the SO-CASPT2 with the ANO-RCC-TZVP Basis Set and Analysis of the Various J -States in Terms of the Dominating LS Terms

exptl [46–48]	ΔE	J -value	weight of LS states
0	0	0	54% 7F , 38% 5D , 7% 3P
2204	1806	1	64% 7F , 32% 5D
4300	4208	2	82% 7F , 17% 5D
6145	6353	3	88% 7F , 10% 5D
7775	8091	4	93% 7F
9179	9552	5	90% 7F
10238	11010	6	85% 7F , 10% 5G
9773	12499	0	44% 7F , 21% 5D , 8% 3P
13528	13612	1	66% 9H , 9% 7F , 7% 7G

the experimental assignments with errors between 91 and 397 cm^{-1} for the first five excited states below 9500 cm^{-1} . Deviations between our results and the available data appear after the sixth state; the experimental assignment predicts the sixth state at 9773 cm^{-1} with a $J = 0$ while such state is found at 12488 cm^{-1} in the current study though uncertainties remain for the attribution of this electronic state. The computed seventh state with $J = 6$ is about 800 cm^{-1} higher energy than the experimental value. Looking closely at the nature of the plutonium low-lying states, one can first notice the remarkable mixing between the 7F , 5D and 3P spin-orbit free states and that the contribution of the 5D state decreases as the energy increases. Finally, the most important result is the overall good reproduction of the SO splitting of 7F spin-free state, making us confident about the accuracy of the SOC for the plutonium molecules. We further note that we have the single-reference $J = 0$ ground state, well described by the ${}^2\text{DC}^{\text{M}}\text{-CCSD(T)}$ method.

For PuO_3 , at the spin-orbit level, we report the description of the ground state and the six lowest excited states in Table IV. It is noteworthy that the $1a_g$, $2a_g/\delta_u$ and $3a_g$ orbitals are doubly occupied in all the calculated spin-free states. The PuO_3 orbitals are composed of a mixture of orbitals belonging to the plutonyl subunit and the distant oxygen. Thus, for the sake of clarity, we label these orbitals with those normally associated to the PuO_2^{2+} ion (with linear energy D_{2h} notations), and those of the distant oxygen atom are denoted by $p_{x,y,z}^{(O)}$. The SO ground state is composed of 47% 3B_2 , 24% 3A_2 and 14% 3B_1 spin-free states. The composition is similar to the one previously reported by Kovács [67] (52% 3B_2 and 24% 3A_2). More striking is the difference between our computed vertical excitation energies with that of Kovács’s SO-CASPT2 spectrum [67].

We predict the first excited state to be at 1235 cm^{-1} , in contrast to the 471 cm^{-1} previously found [67], and the overall spectrum determined from our calculations is much denser and lower by about 4000 cm^{-1} than in ref. [67]. Such discrepancy may find its origin in the description of the spin-free states. Although we agree with Kovács that the spin-free ground state has 3B_2 symmetry, we find a different orbital character. In our calculations, the 3B_2 exhibits a strong multideterminantal character with 57% corresponding to the configuration in which the $4a_1/p_z^{(O)}$ and $2b_2/\sigma_u$ orbitals are doubly occupied (See Table IV and Figure 1) and the singly occupied orbitals $5b_1/\Phi_u$, $1b_2/p_z^{(O)}$, $3b_2/\delta_u$ and $1a_2/\delta_u$ and 22% from the electronic configuration in which of the $4a_1/p_z^{(O)}$, $1b_2/p_z^{(O)}$ and $2b_2/\sigma_u$ orbitals are doubly occupied and the $5b_1/\Phi$ and $1a_2/\delta_u$ singly occupied. Kovács, however, finds the ground state to be mainly composed of plutonyl orbitals (79%).

Such a difference can be explained by the fact that the considered active spaces are different, a CAS(10,16) in his case and a CAS(14,13) in our work. In a close look at the entanglement diagram of PuO_3 derived from DMRG calculations [10] (Figure 6a, Full-Valence CAS) there is a strong correlation within the nonbonding plutonyl-like orbitals (δ_u, ϕ_u) and also between the $b_2/p^{(O)}$ and the

PuO_3 and $\text{PuO}_2(\text{OH})_2$ molecules

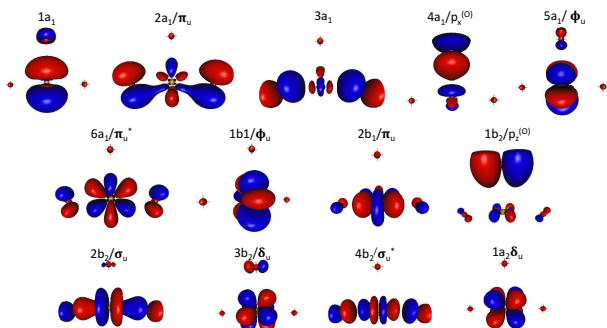


FIG. 1: Active CASSCF orbitals of PuO_3 at the CASSCF level; Isosurface = 0.05 ua; Distances: $\text{Pu-O}(\text{PuO}_2^{2+}\text{subunit}) = 1.767 \text{ \AA}$; $\text{Pu-O}_{axial} = 1.934 \text{ \AA}$; angle (O-Pu-O_{axial}) = 93.86°

TABLE IV: Lowest Vertical Transition Energies (ΔE in cm^{-1}) of PuO_3 Computed at the SF-CASPT2 and SO-CASPT2 Levels with the ANO-RCC-TZVP Basis Set and Analysis of the Various States

no. state	ΔE	character : % [orbital(number of electron)]
SF 1 $^3B_2(1)$	0	36% $[4a_1/p^{(O)}(2), 1b_1/\phi_u(1), 1b_2/p^{(O)}(\bar{1}), 2b_2/\sigma_u(2), 3b_2/\delta_u(1), 1a_2/\delta_u(1)]$ 21% $[4a_1/p^{(O)}(2), 1b_1/\phi_u(1), 1b_2/p^{(O)}(1), 2b_2/\sigma_u(2), 3b_2/\delta_u(\bar{1}), 1a_2/\delta_u(1)]$ 22% $[4a_1/p^{(O)}(2), 1b_1/\phi_u(1), 1b_2/p^{(O)}(2), 2b_2/\sigma_u(2), 1a_2/\delta_u(1)]$
2 $^3A_2(1)$	3161	43% $[4a_1/p^{(O)}(2), 5a_1/\phi_u(1), 1b_2/p^{(O)}(\bar{1}), 2b_2/\sigma_u(2), 3b_2/\delta_u(1), 1a_2/\delta_u(1)]$ 23% $[4a_1/p^{(O)}(2), 5a_1/\phi_u(1), 1b_2/p^{(O)}(1), 2b_2/\sigma_u(2), 3b_2/\delta_u(\bar{1}), 1a_2/\delta_u(1)]$ 17% $[4a_1/p^{(O)}(2), 5a_1/\phi_u(1), 1b_2/p^{(O)}(2), 2b_2/\sigma_u(2), 1a_2/\delta_u(1)]$
3 $^3B_1(1)$	4663	38% $[4a_1/p^{(O)}(2), 5a_1/\phi_u(1), 1b_1/\phi_u(1), 1b_2/p^{(O)}(\bar{1}), 2b_2/\sigma_u(2), 3b_2/\delta_u(1)]$ 12% $[4a_1/p^{(O)}(2), 5a_1/\phi_u(1), 2b_1/\pi_u(1), 1b_2/p^{(O)}(\bar{1}), 2b_2/\sigma_u(2), 3b_2/\delta_u(1)]$ 12% $[4a_1/p^{(O)}(2), 5a_1/\phi_u(1), 1b_1/\phi_u(1), 2b_1/\pi_u(2), 1b_2/p^{(O)}(2)]$
4 $^1A_1(1)$	7239	32% $[4a_1/p^{(O)}(2), 1b_2/p^{(O)}(1), 2b_2/\sigma_u(2), 3b_2/\delta_u(\bar{1}), 1a_2/\delta_u(2)]$ 28% $[4a_1/p^{(O)}(2), 1b_2/p^{(O)}(2), 2b_2/\sigma_u(2), 1a_2/\delta_u(2)]$ 11% $[4a_1/p^{(O)}(1), 5a_1/\Phi_u(\bar{1}), 1b_2/p^{(O)}(2), 2b_2/\sigma_u(2), 1a_2/\delta_u(2)]$
5 $^3A_2(2)$	7287	20% $[4a_1/p^{(O)}(2), 1b_1/\phi_u(1), 1b_2/p^{(O)}(1), 2b_2/\sigma_u(2), 3b_2/\delta_u(2)]$ 18% $[4a_1/p^{(O)}(1), 5a_1/\Phi_u(\bar{1}), 1b_1/\phi_u(1), 1b_2/p^{(O)}(2), 2b_2/\sigma_u(2), 3b_2/\delta_u(1)]$ 17% $[4a_1/p^{(O)}(2), 1b_1/\phi_u(1), 1b_2/p^{(O)}(2), 2b_2/\sigma_u(2), 3b_2/\delta_u(1)]$
6 $^3B_1(2)$	8038	31% $[4a_1/p^{(O)}(1), 5a_1/\Phi_u(\bar{1}), 1b_2/p^{(O)}(2), 2b_2/\sigma_u(2), 3b_2/\delta_u(1), 1a_2/\delta_u(1)]$ 11% $[4a_1/p^{(O)}(2), 5a_1/\phi_u(1), 2b_1/\pi_u(1), 1b_2/p^{(O)}(\bar{1}), 2b_2/\sigma_u(2), 3b_2/\delta_u(1)]$ 10% $[4a_1/p^{(O)}(2), 1b_2/p^{(O)}(2), 2b_2/\sigma_u(2), 3b_2/\delta_u(1), 1a_2/\delta_u(1)]$ 10% $[4a_1/p^{(O)}(2), 1b_1/\phi_u(1), 2b_1/\pi_u(1), 1b_2/p^{(O)}(\bar{1}), 2b_2/\sigma_u(2), 1a_2/\delta_u(1)]$
SO X	0	47% $^3B_2(1)$ + 24% $^3A_2(1)$ + 14% $^3B_1(1)$
a	1235	59% $^3B_2(1)$ + 25% $^3A_2(1)$
b	1783	73% $^3B_2(1)$
c	3777	51% $^3A_2(1)$
d	5660	24% $^3B_1(1)$ + 18% $^1A_1(1)$ + 17% $^3A_2(2)$ + 10% $^3B_1(2)$

$5f\delta_u$ orbitals, in agreement with our analysis of the 3B_2 ground-state wave function.

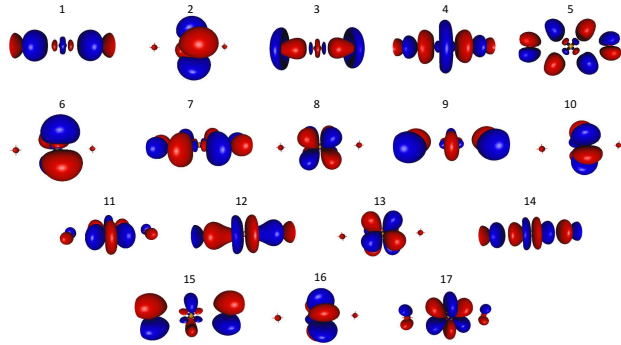


FIG. 2: Molecular orbitals of $\text{PuO}_2(\text{OH})_2$ at CASSCF level. Isosurface = 0.05 ua; Distances: Pu-OH = 2.103 Å, Pu-O = 1.742 Å; Angles: O-Pu-OH = 92.15°; HO-Pu-OH = 105.68°; O-Pu-O = 174.29°.

Concerning $\text{PuO}_2(\text{OH})_2$, the low-energy part of the vertical spectrum including SOC reported in the Table V shows two close-lying states separated by about 323 cm^{-1} , followed by a state at 2222 cm^{-1} . The analysis of the two lowest states indicates that they correspond to a 50-50 combination of $(1)^3A$ and $(1)^3B$ spin-free states, with a small contribution of the $(2)^3B$ (6% in each case). The next three states also have strong mixings induced by SOC between triplet states but also singlet excited states of $(1)^1A$ and $(1)^1B$ symmetries, placed at the spin-free

level at about 5764 and 7444 cm^{-1} , respectively.

PuO_2 and PuO_2^+ Molecules

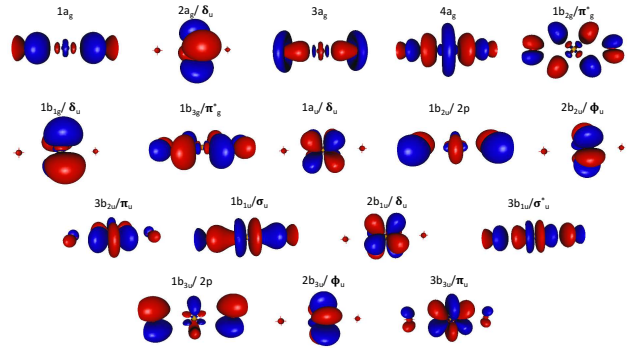


FIG. 3: Molecular orbitals of PuO_2 at the CASSCF level; $r(\text{Pu}-\text{O})=1.808 \text{ Å}$; Isosurface = 0.05 ua.

At the $^2\text{DC}^M$ level, the PuO_2 ground state is found to be well-described by a closed-shell ($\Omega = 0_g^+$) determinant, corresponding to occupied $5f_{-3/2;+3/2}$, $5f_{-5/2;+5/2}$ spinors. We note that the T_1 diagnostic is 0.03, a value very similar to that found for single-reference uranium molecules [16]. This allowed us to employ accurate two-component single-reference approaches such as CCSD(T) to determine the optimal Pu-O bond length after CBS extrapolation to be 1.808 Å , with a correspond-

TABLE V: Lowest Vertical Transition Energies (ΔE in cm^{-1}) of $\text{PuO}_2(\text{OH})_2$, Computed at the SF-CASPT2 and SO-CASPT2 Levels with ANO-RCC-TZVP Basis Sets and Analysis of the Various States

state	ΔE	character : % [orbital(number of electron)]
SF (1) ³ B	0	49% [2a/ $\phi_u(1)$, 1b/ $\delta_u(1)$] 48% [1a/ $\delta_u(1)$, 2b/ $\phi_u(1)$]
(1) ³ A	889	41% [1a/ $\delta_u(1)$, 2a/ $\phi_u(1)$] 59% [1b/ $\delta_u(1)$, 2b/ $\phi_u(1)$]
(2) ³ B	2136	75% [1a/ $\delta_u(1)$, 1b/ $\delta_u(1)$] 20% [2a/ $\phi_u(1)$, 2b/ $\phi_u(1)$]
(2) ³ A	4698	59% [1a/ $\delta_u(1)$, 2a/ $\phi_u(1)$] 41% [1b/ $\delta_u(1)$, 2b/ $\phi_u(1)$]
(3) ³ B	5351	52% 2a/ $\phi_u(1)$, 1b/ $\delta_u(1)$ 46% [1a/ $\delta_u(1)$, 2b/ $\phi_u(1)$]
(1) ¹ A	5764	[58% 1b/ $\delta_u(1)$, 2b/ $\Phi_u(\bar{1})$] 30% [1a/ $\delta_u(1)$, 2a/ $\Phi_u(\bar{1})$] 5%[2a/ $\phi_u(2)$]
(1) ¹ B	7444	50% [1a/ $\delta_u(1)$, 1b/ $\delta_u(\bar{1})$] 28% [2a/ $\phi_u(1)$, 2b/ $\Phi_u(\bar{1})$] 16%[1a/ $\delta_u(1)$, 2b/ $\Phi_u(\bar{1})$]
(2) ¹ A	9626	39% [1a/ $\delta_u(1)$, 2a/ $\Phi_u(\bar{1})$] 29 % [2a/ $\phi_u(2)$] 13% [1b/ $\delta_u(1)$, 2b/ $\Phi_u(\bar{1})$] 10% [1a/ $\delta_u(2)$] 7 % [2a/ $\phi_u(2)$]
SO X	0	46% (1) ³ A, 41% (1) ³ B, 6% (2) ³ B
a	323	45.% (1) ³ B, 45% (1) ³ A, 6% (2) ³ B
b	2222	35% (2) ³ B, 25% (1) ³ B, 14% (1) ¹ A, 13% (2) ³ A, 10% (3) ³ B
c	3757	40% (2) ³ A, 25% (2) ³ B, 19% (1) ¹ B, 7% (1) ³ B, 6% (1) ³ A
d	4158	36% (3) ³ B, 34% (2) ³ B, 14% (2) ¹ A, 11% (1) ³ B,

TABLE VI: Comparison of CBS Extrapolated ²DC^M-EOM-CCSD and SO-CASPT2 PuO_2 Vertical Transition Energies (ΔE in cm^{-1}) Computed at the 1.744 and 1.808 Å Pu–O Distances

Ω	d(Pu-O)=1.744 Å			d(Pu-O)=1.808 Å	
	² DC ^M -EOM-CCSD ΔE	SO-CASPT2 ΔE	ΔE [51]	² DC ^M -EOM-CCSD ΔE	SO-CASPT2 ΔE
0 _g ⁺	0	0	1794	0	0
1 _g	2554	1438	2315	2457	2462
2 _g	6366	4235	4131	5663	5904
0 _g	7138			7134	
3 _g	9480			9073	
1 _g	10 098			9502	
0 _g	10 195			10 415	
1 _u	7011	1778	0	9822	5851
2 _u	7225	1805	535	10 057	6265
2 _u	7653			10 854	
3 _u	7955			11 214	
4 _u	13 531			16 236	

ing harmonic vibrational symmetric stretching frequency of 791 cm^{-1} (the anti-symmetric stretch and bending frequencies being 840 and 170 cm^{-1} , respectively). We note that these results are in excellent agreement with the scalar relativistic CCSD(T) geometry (1.814 \AA) and harmonic frequencies ($147, 777, 825 \text{ cm}^{-1}$) reported by Feng and Peterson [68], who agree with us that PuO_2 ground state has a 0_g^+ character with a longer distance than the

one (1.744 \AA) predicted by La Macchia et al. [51, 69] at the SO-CASPT2 level, though for chemically different ground state $^5\Phi_u$.

Furthermore, our ²DC^M-EOM-EE-CCSD calculations (see Table VI) confirm that, at the CBS-²DC^M-CCSD(T) equilibrium structure, the $\Omega = 0_g^+$ state is indeed the ground state: it is sufficiently well-separated from the lowest-lying states of both g ($\Omega = 1_g$, by over 2000 cm^{-1})

and u ($\Omega = 1_u$, by over 5000 cm^{-1}), and considering a shorter bond length, namely 1.744 \AA , as was proposed by La Macchia et al. [51] for the ground state from SO-CASPT2 calculations, does not alter this picture. Thus, our results differ qualitatively and quantitatively from ref. 51, which found the PuO_2 ground state to be of $\Omega = 1_u$ symmetry, corresponding to the occupation of the two δ_u , one ϕ_u and the $7s$ orbitals (See Figure 3).

From Table VI, we observe significant variations for the u-states (of nearly 3000 cm^{-1}) when the internuclear distance is shortened from 1.808 \AA to 1.744 \AA , while the g-states remain more or less at the same energies. With this, at this longer distance, the $\Omega = 2_g$ state becomes lower than the $\Omega = 1_u$ state.

The SO-CASPT2 transition energies computed at the $^2\text{DC}^{\text{M}}$ optimal bond length are reported in Tables VI and VII and Table S5 in the Supporting Information. The spin-orbit 0_g^+ ground state is composed by the spin-free ground state $(1)^5\Sigma_g^+$ up to 48% and by the $^3\Sigma_g^-(1)$ up to 22%, which lies 10308 cm^{-1} above it. Note that the current vertical transition energies computed at the SO-CASPT2 level are in very good agreement with the $^2\text{DC}^{\text{M}}$ energies for the g-states, but the u-manifold come out about 4000 cm^{-1} lower in energy at the SO-CASPT2 level than at the $^2\text{DC}^{\text{M}}$ -EOM-CCSD level. The fact that the $0_g^+ - 1_u$ energy difference computed at the SO-CASPT2 level of theory (5851 cm^{-1}) agrees best with the spin-orbit corrected CCSD(T) value by Feng and Peterson (5421 cm^{-1}) than with the $^2\text{DC}^{\text{M}}$ -EOM-CCSD value, suggests that triple corrections have a large contribution to such g to u transitions involving a change in Pu orbital occupations. Thus, all levels of theory predict the ground state to have 0_g^+ symmetry at both shorter and longer Pu-O distances, disagreeing with the proposed 1_u nature of the ground state by La Macchia et al. [51]. However, we note that the electronic state spacing within either the g or u symmetries agrees in both SO-CASPT2 calculations. This finding points out to the importance of the choice of the active space to accurately predict the relative energies of g-states involving mostly nonbonding $5f$ Pu atomic-centered orbitals, versus the u-states involving the more diffuse Pu $7s$ orbital.

Beside calculations including SOC, it is informative to discuss the nature of the PuO_2 ground-state without SOC. Our CASPT2 and UCCSD(T) calculations place the $^5\Sigma_g^+$ state ($(\delta_u)^2(\phi_u)^2$ occupations) lower in energy than the $^5\Phi_u$ state ($(\delta_u)^2(\phi_u)^1(7s)^1$) by 7994 cm^{-1} at a Pu-O distance of 1.808 \AA , as found in the previous studies [51, 70]. With the ANO-RCC AVTZ basis set, the equilibrium Pu-O distances are 1.818 and 1.808 \AA at the UCCSD(T) and CASPT2 levels, respectively, distances that are close to the $^2\text{DC}^{\text{M}}$ -CCSD(T) result. These values are also in line with the SF-CASPT2 (CAS(12,14)) of La Macchia ($d(\text{Pu-O}) = 1.792 \text{ \AA}$), but significantly shorter (by about $0.04/0.05 \text{ \AA}$) than the estimations of Archibong and Ray [70]. The large discrepancies ob-

served with respect to the latter are probably related to the choice of a large-core RECP (78 electrons), which yields bond distances in actinide molecules that are too long [71], while the small-core ECP gives exactly the same distances as the all-electron Douglas-Kroll relativistic approach.

The ground state $(1)^5\Sigma_g^+$ is dominated (84%) by the configuration in which the two $5\delta_u$ and two ϕ_u orbitals carry one electron each. It corresponds to the description of the ground state of Boguslawski et al. [10] and by Feng and Peterson [68], and also to the $(1)^5\Sigma_g^+$ state reported by La Macchia et al. [51]. The former study places the first excited state at 1800 cm^{-1} corresponding to $^5\Phi_u$ state, while in our SF-CASPT2 calculation it appears at a higher energy (5421 cm^{-1}). We note that in our SF-CASPT2 calculation the spectrum is less dense than in La Macchia's results [51]. Such differences can be explained by the choice of different active spaces, by the fact that we computed a larger number of spin-free states, and most likely by the change in the interatomic Pu-O distance. SOC is not expected to change the energy of the $\Omega = 0_g^-$ state, while it lifts the degeneracy of the $^5\Phi_u$ state, giving rise to three (1_u , 2_u , and 3_u) fine structure states, split by 2133 cm^{-1} (See Table 4 of ref. 51). Given the small energy gap of 1800 cm^{-1} in La Macchia's [51] study between the $^5\Sigma_g^+$ and $^5\Phi_u$ states, the 1_u state becomes the ground state, while in our work, it remains a state of *gerade* symmetry (0_g^+), unambiguously confirmed by the $^2\text{DC}^{\text{M}}$ calculations.

Apart from determining the excitation energies for PuO_2 , the EOM-CCSD method is also useful to investigate the ionization potentials of PuO_2 , for which there are experimental data. Being a relative measure, this can help to validate $^2\text{DC}^{\text{M}}$ -EOM-CCSD as a reliable approach with which to benchmark SO-CASPT2. The computed vertical and adiabatic ionization energies (IP; see Table VIII) can be grouped into three regions with respect to their energies: two below 8 eV , one between 8 and 10 eV and the last at energies higher than 10 eV . The lowest EOM-IP-CCSD state has $\Omega = 3/2_u$ symmetry, as found by Feng and Peterson [68], with an adiabatic IP of 7.07 eV , in very good agreement with the SO-CCSD(T) value (6.93 eV) [68], and within the error bar of the adiabatic value ($7.03 \pm 0.12 \text{ eV}$, measured by Santos et al. [23]) However, the values reported by Rauh et al. [20] and Capone et al. [22], lying at 9.4 ± 0.5 and $(10.1 \pm 0.1) \text{ eV}$, respectively would match the value we computed for the first $\Omega = 1/2_u$, leading us to suggest that these experiments may have measured PuO_2^+ in different electronically excited states.

The calculated electronic states of PuO_2^+ correspond to ionizations from the nonbonding δ_u ($\Omega = 3/2_u$) and ϕ_u ($\Omega = 5/2_u$), and from the bonding σ_u ($\Omega = 1/2_u$) and π_u ($\Omega = 3/2_u$). In the first two cases, as we do not alter the number of bonding spinors, the removal of an electron increases the Pu-O bond energy, as can be seen by the

TABLE VII: Lowest Vertical Transition Energies (ΔE in cm^{-1}) of PuO_2 Computed at the SF-CASPT2 and SO-CASPT2 Levels ($d(\text{Pu-O})=1.808 \text{ \AA}$) with ANO-RCC-TZVP Basis Sets and Analysis of the Various States

state	ΔE	character : % [orbital(number of electron)]
SF (1) $^5\Sigma_g^+$	0	84% [1a _u / δ_u (1), 2b _{2u} / ϕ_u (1), 2b _{1u} / δ_u (1), 2b _{3u} / ϕ_u (1)]
(1) $^5\Sigma_g^-$	4798	45% [1a _u / δ_u (1), 3b _{2u} / π_u (1), 2b _{1u} / δ_u (1), 2b _{3u} / ϕ_u (1)] 45% [1a _u / δ_u (1), 2b _{2u} / ϕ_u (1), 2b _{1u} / δ_u (1), 3b _{3u} / π_u (1)]
(1) $^5\Phi_u$	5421	85% [3a _g (1), 1a _u / δ_u (1), 2b _{1u} / δ_u (1), 2b _{3u} / ϕ_u (1)]
(1) $^5\Delta_u$	7452	79% [3a _g (1), 2b _{2u} / ϕ_u (1), 2b _{1u} / δ_u (1), 2b _{3u} / ϕ_u (1)]
(1) $^3\Sigma_g^-$	10308	24% [1a _u / δ_u (1), 2b _{2u} / ϕ_u (2), 2b _{1u} / δ_u (1)] 24% [1a _u / δ_u (1), 2b _{1u} / δ_u (1), 2b _{3u} / ϕ_u (2)] 19% [2b _{2u} / ϕ_u (1), 2b _{1u} / δ_u (2), 2b _{3u} / ϕ_u (1)] 16% [1a _u / δ_u (1), 2b _{2u} / ϕ_u (1), 2b _{3u} / ϕ_u (1)]
SO 0 $_g^+$	0	48% (1) $^5\Sigma_g^+$, 22% (1) $^3\Sigma_g^-$
1 $_g$	2462	67% (1) $^5\Sigma_g^+$, 15% (1) $^3\Sigma_g^-$
1 $_u$	5851	27% (1) $^5\Phi_u$, 27% 21% (2) $^5\Phi_u$, 13% (1) $^5\Delta_u$, 13% (2) $^5\Delta_u$
2 $_g$	5904	85% (1) $^5\Sigma_g^+$
2 $_u$	6265	21% (1) $^5\Phi_u$, 21% (2) $^5\Phi_u$, 24% (1) $^5\Delta_u$
3 $_u$	7195	39% (1) $^5\Phi_u$, 25% (2) $^5\Phi_u$

TABLE VIII: CBS Extrapolated Vertical and Adiabatic Ionization Potentials (IPs in eV) of PuO_2 Computed at the $^2\text{DC}^{\text{M}}$ -EOM-IP-CCSD Level. The interatomic distance ($r_e(\text{Pu-O})= 1.808 \text{ \AA}$, from $^2\text{DC}^{\text{M}}$ -CCSD(T) calculations) was used for the vertical IPs, while the adiabatic IPs correspond to the reported equilibrium r_e distances of PuO_2^+ and harmonic symmetric stretching ω_e frequencies. Experimental and other theoretical values correspond to adiabatic IPs

State	$^2\text{DC}^{\text{M}}$ -EOM-IP-CCSD			
	IP _{vert}	IP _{adiab}	r_e	ω_e
3/2 $_u$	7.67	7.07	1.697	1010
5/2 $_u$	7.93	7.20	1.688	1035
1/2 $_u$	9.81	9.77	1.771	811
3/2 $_u$	10.80	10.79	1.831	940
		Theor. (IP _{adiab})		
X2C-DC-CCSD(T)		5.93	ref. 69	
SO-CCSD(T)		6.93	ref. 68	
		Exp (IP _{adiab})		
		9.4 \pm 0.5	ref. 20	
		10.1 \pm 0.1	ref. 22	
		7.03 \pm 0.12	ref. 23	
		6.6 ^a	refs. 72, 73	

^a Rejected value according to the comment by Gibson et al. [73] on Capone et al.'s measurements [72].

decreased equilibrium bond length and higher harmonic vibrational stretching frequencies compared to the CCSD values ($r_e(\text{Pu-O})=1.792 \text{ \AA}$; $\omega_e=833 \text{ cm}^{-1}$) for PuO_2 (by about 0.095 \AA and 177 cm^{-1} for $\Omega = 3/2_u$, and 0.104 \AA and 202 cm^{-1} for $\Omega = 5/2_u$).

The other two states, on the other hand, can be seen as excited states where the electrons from the bonding σ_u and π_u spinors are excited to the nonbonding δ_u and as such the net bonding interaction is reduced in the molecule, whereas for the second $\Omega = 3/2_u$ there is an increase in bond length and in frequency in comparison to the PuO_2 CCSD(T) values (by 0.039 \AA and 107 cm^{-1}). Finally, for the $\Omega = 1/2_u$, we observe a slight decrease in bond length (of 0.021 \AA) together with a slight decrease in vibrational frequency (of 21 cm^{-1}) in comparison to the PuO_2 CCSD(T) values.

Taken together our $^2\text{DC}^{\text{M}}$ -EOM-CCSD calculations show it can be used to assess the SO-CASPT2 method for energy differences.

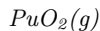
Thermodynamic Data

All of the results so far have demonstrated the accuracy and reliability of the $^2\text{DC}^{\text{M}}$ -CCSD approach and the relative accuracy of SO-CASPT2. Now, we can proceed with the determination of the thermodynamic data. Recently, a thorough assessment of the thermodynamic properties of gaseous plutonium oxides has been done by Konings et al. [2]. The derived functions (entropy and heat capacity) have been calculated on the basis of the most reliable data available in the literature. Nev-

ertheless, the authors pointed out a number of missing data, especially regarding the contributions of electronically excited states.

In the following, from results discussed before and the related molecular parameters and electronic states (see Tables S7–S9 in the Supporting Information), the heat capacity and the standard entropy of $\text{PuO}_2(\text{g})$, $\text{PuO}_3(\text{g})$ and $\text{PuO}_2(\text{OH})_2(\text{g})$ are thus derived and compared to those selected by Konings et al. [2] or calculated by Ebbinghaus [74]. Regarding the standard heat of formation, an analysis of transpiration measurements made by Krikorian et al. [5] was performed to extract values of $\text{PuO}_3(\text{g})$ and $\text{PuO}_2(\text{OH})_2(\text{g})$, whereas for $\text{PuO}_2(\text{g})$, our results are analyzed in the light of Konings’ assessment [2].

From the discussions on the previous sections of the electronic structures of the different Pu species, one will not be surprised to see that the single-reference methods, DFT and CC, fail at describing standard heats of formation of $\text{PuO}_2(\text{OH})_2$ and PuO_3 , while it should be in principle applicable for PuO_2 . For the latter, data obtained by coupled-cluster calculations are therefore used to establish its thermodynamic properties whereas regarding the other species, multireference results are used.



Let us first discuss the thermodynamic functions of PuO_2 . Regarding the standard entropy at room temperature, an analysis of the sources of discrepancies between our calculation and up-to-date data from the literature reveals that vibrational and electronic partition functions are in disagreement (see Table S10 in the Supporting Information).

In the thermodynamic review of Konings et al. [2], although information on the PuO_2 electronic states could have been taken from La Macchia et al. [51], the contributions to the entropy of the PuO_2 electronic states were estimated by considering the crystal-field split $5f^2$ energy levels of $\text{PuF}_4(\text{cr})$, which are densely spaced, thus leading to a significant overestimation of the electronic contributions to entropy. Regarding the vibrational contributions, Konings et al. [2] used the harmonic frequencies computed at the scalar relativistic CCSD(T) level by Archibong and Ray [70]. Our ${}^2\text{DC}^{\text{M}}\text{-CCSD(T)}$ harmonic stretching frequencies (791 and 840 cm^{-1}) are very close to their CCSD(T) values (792 and 828 cm^{-1}) and to the DKH3-CCSD(T) values of Feng and Peterson [68] (777 and 825 cm^{-1}), the bending frequency comes out slightly higher in our calculation (170 cm^{-1}) than in previous reports (106 cm^{-1} [70], and 147 cm^{-1} [68]), probably due to the inclusion of spin-orbit coupling. As a result our thermodynamics function differs from that proposed by Konings et al. [2] Unfortunately, except for the asymmetric stretching mode by infrared absorption spectroscopy [75]

of PuO_2 in Ar and Kr matrices (794.25 and 786.80 cm^{-1}), the other vibrational frequencies are unknown, making it impossible to assess the accuracy of the currently reported quantum chemical frequencies. Our calculated standard entropy at room temperature is thus equal to

$$S_{298\text{ K}}^{\ominus} = 262.9\text{ J K}^{-1}\text{ mol}^{-1}, \quad (6)$$

which is lower by about $16\text{ J K}^{-1}\text{ mol}^{-1}$ than the value in the assessment of Konings et al. ($278.7\text{ J K}^{-1}\text{ mol}^{-1}$) [2]. An analogous discussion can be made as to the effect of the PuO_2 electronic states on the heat capacity (see Figure S1 in the Supporting Information). At room temperature, Konings et al. [2] reported a $C_p^{\ominus}(T)$ value higher than ours by tens of $\text{J K}^{-1}\text{ mol}^{-1}$, due to their overestimated excited-state contributions. The heat capacity function of the present work (in $\text{J K}^{-1}\text{ mol}^{-1}$) is expressed as

$$C_p^{\ominus}(T) = 42.7970 + 3.5713 \times 10^{-2}(T/K) - 1.2077 \times 10^{-5}(T/K)^2 - 2.0271 \times 10^5(T/K)^{-2} \quad (7)$$

in the 298.15–1200 K temperature range, and becomes:

$$C_p^{\ominus}(T) = 54.1604 + 1.2436 \times 10^{-2}(T/K) - 1.7456 \times 10^{-6}(T/K)^2 + 2.2335 \times 10^6(T/K)^{-2} \quad (8)$$

in the 1200–3000 K range.

Coming now to the standard enthalpy of formation of PuO_2 , we first note that the value we report in Table IX from B3LYP calculations including the spin-orbit $+\Delta E_{\text{SO}}$ correction is about 25% off (100 kJ mol^{-1}) the experimental value. A change in the density functional will not ensure a better agreement with experiment as observed previously for actinide systems [76] or for transition metal molecules [77]. Thus, we will rely on wavefunction-based approaches to propose revised values of $\Delta_f H^{\ominus}(298.15\text{ K})$, and will take the CBS corrected ${}^2\text{DC}^{\text{M}}\text{-CCSD(T)}$ result to be the best estimate for the standard heat of formation of $\text{PuO}_2(\text{g})$, yielding

$$\Delta_f H^{\ominus}(298.15\text{ K}) = (-449.5 \pm 8.8)\text{ kJ mol}^{-1}. \quad (9)$$

In addition, by combining the ${}^2\text{DC}^{\text{M}}\text{-CCSD(T)}$ standard enthalpy of formation of PuO_2 with the ${}^2\text{DC}^{\text{M}}\text{-EOM-IP-CCSD}$ value of its adiabatic ionization potential $\text{IE}(\text{PuO}_2)$, we can predict the standard enthalpy of formation of PuO_2^+ through the relation

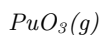
$$\begin{aligned} \Delta_f H^{\ominus}[\text{PuO}_2^+] &= \Delta_f H^{\ominus}[\text{PuO}_2] + \text{IE}[\text{PuO}_2] + H^{\ominus}(298.15\text{ K})[\text{PuO}_2^+] \\ \Delta_f H^{\ominus}[\text{PuO}_2^+] &= (234.9 \pm 8.8)\text{ kJ mol}^{-1}. \end{aligned} \quad (10)$$

The SO-UCCSD(T) value ($(-411.2 \pm 6.6)\text{ kJ mol}^{-1}$) for $\Delta_f H^{\ominus}[\text{PuO}_2]$ roughly agrees with both the latter and experiment, but it is lower than the CBS- ${}^2\text{DC}^{\text{M}}\text{-CCSD(T)}$ value ($(-449.5 \pm 8.8)\text{ kJ mol}^{-1}$) by about

38 kJ mol⁻¹. The importance of the perturbative triple contributions in the electronic correlation treatment is highlighted by comparing these results to the CCSD results (see Table IX), as the one-step and two-step models show differences of 40 and 58 kJ mol⁻¹, respectively. The difference between the SO-UCCSD(T) and ²DC^M-CCSD(T) methods could be explained by a possible underestimation of the SOC contribution in the two-step approach, yielding a $\Delta_f H^\ominus(298.15\text{ K})$ value higher by about 30 kJ mol⁻¹. The SO-CASPT2 value ($\Delta_f H^\ominus(298.15\text{ K}) = (-413.7 \pm 18.3)$ kJ mol⁻¹) reported in Table IX deviates by about 36 kJ mol⁻¹ from both ²DC^M-CCSD(T) and experiments and by about 2 kJ mol⁻¹ from the SO-UCCSD(T) value, therefore showing a fair agreement with the most accurate methods. This is mirrored in the closeness of the PuO₂ atomization energies (reverse of reaction R2), reported in Table S11 in the Supporting Information. With this we concluded that perturbative approaches (²DC^M-CCSD(T) and SO-CASPT2) yield reasonable results, and thus could be used for other systems, though with larger uncertainties for SO-CASPT2 than for ²DC^M-CCSD(T).

Going back to the available literature data, the $\Delta_f H^\ominus(298.15\text{ K})$ computed with the ²DC^M-CCSD(T) approach is in almost perfect agreement with the available results that correspond to the highest values for the formation enthalpy in Table IX [2, 78]. The SO-CASPT2(4,4) value exhibits a rather good agreement with the selected one in the Konings assessment [2] (the value has been obtained by a second law method applied to experiments published in ref. [78]). This is motivated by the statement that the values obtained by third or second law analysis are not fully in agreement [2, 78] revealing a lack of consistency of experimental data.

Therefore, in future studies, experimental data can be scrutinized in regard to the present thermodynamic functions of PuO₂. The crosscheck between data from molecular parameters and standard heat of formation from quantum chemistry calculations as well as values from experiments calls for further assessments.



As highlighted in the case of the PuO₂(g) molecule, the uncertainties related to the entropy and heat capacity functions stem from the electronic partition functions. Ebbinghaus [74] and Konings et al. [2], both used the electronic spectra of PuO₂²⁺ to estimate that of PuO₃ [8, 79]. The latter approximation is found here to be strong, even if both our calculations and the studies by Konings et al. [2] and Ebbinghaus [74] consider that the ground state is dominated by triplet spin-free states. Indeed, while Konings et al. only considered four states from the calculations of Infante et al.'s calculations [8], we find seven states below 8000 cm⁻¹.

Regarding the vibrational contributions, the estimate used by these authors and based on an analogy with UO₃(g), seems to be acceptable because of a fortuitous good agreement, as highlighted by our calculations. The improvements of the electronic partition function lead to a weak decrease (see Table S10 in the Supporting Information) of the standard entropy at room temperature, and is thus equal to

$$S_{298\text{ K}}^\ominus = 310.98 \text{ J K}^{-1} \text{ mol}^{-1}, \quad (11)$$

and the heat capacity function of PuO₃(g) (in J K⁻¹ mol⁻¹) is

$$C_p^\ominus(T) = 43.0757 + 1.0927 \times 10^{-1}(T/K) - 7.1581 \times 10^{-5}(T/K)^2 - 7.1469 \times 10^4(T/K)^{-2} \quad (12)$$

for the 298.15–550 K temperature range, and

$$C_p^\ominus(T) = 98.1101 - 1.1768 \times 10^{-2}(T/K) + 4.5533 \times 10^{-6}(T/K)^2 - 3.5486 \times 10^6(T/K)^{-2}. \quad (13)$$

in the 550–2400 K range.

The only available experimental data of PuO₃(g) for which its standard heat of formation has been obtained comes from the transpiration method of plutonium oxide under an oxygen atmosphere [5]. The involved species is postulated from an analogy with uranium, and under the experimental conditions (under a purely oxygen flow), PuO₃ is expected to be the major volatile species (under a purely oxygen flow). In this type of apparatus, the partial pressure of target species is obtained by an indirect method (measure of transported masses), which may cause a bias in the present case due to a potential contamination of the results by the ash transport (pointed out by the authors of ref. 80). Nevertheless, one set of measures has been obtained with another apparatus configuration in which a silica wool glass filter has been added between the crucible and the collector tube (in a region where the temperature remains high).

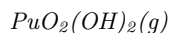
Strangely, these obtained data are excluded because the following postulate has been made by authors: the lowest plutonium volatility is due to an interaction between its vapor and silica wool. Therefore, the standard heat of formation retained by the authors (-562.8 kJ mol⁻¹) [5] has been obtained with the set without a silica wool filter. However, one can make the assumption that the filter traps the ash. As the filter is located in a hot zone, in the vicinity of the crucible, one can postulate that only vapor species pass through the filter without modifying the equilibrium. Thus, the data set obtained with a filter may be more accurate than that without a silica wool filter.

Taking advantage of our improved entropy and heat capacity for the PuO₃ molecule, we can reanalyze the

experimental data using our *ab initio* data. The treatments by the third law method with the proper Gibbs energy functions of $\text{PuO}_2(\text{c})$ [2] and one from our adopted data for $\text{PuO}_3(\text{g})$ lead to the following $\Delta_f H^\ominus$ values: $(-572.0 \pm 12.1) \text{ kJ mol}^{-1}$ from the data set without a silica wool filter and $(-534.0 \pm 18.5) \text{ kJ mol}^{-1}$ with it [81]. The former slightly differs from the original value $(-562.8 \text{ kJ mol}^{-1})$ [5], due to our improvement of the standard entropy for $\text{PuO}_3(\text{g})$. We propose that the standard heat of formation computed within the SO-CASPT2 approach can be considered as the best estimated data

$$\Delta_f H^\ominus(298.15 \text{ K}) = (-553.2 \pm 27.5) \text{ kJ mol}^{-1}. \quad (14)$$

The predicted theoretical $\Delta_f H^\ominus(298.15 \text{ K})$ is in the same range as the values reported in Table IX and is in agreement with the new assessments of experimental data proposed here.



Ebbinghaus' work reports the evaluation of the entropy and heat capacity of the plutonium oxy-hydroxide [74]. To compute the electronic contribution to the thermodynamics function of $\text{PuO}_2(\text{OH})_2(\text{g})$, Ebbinghaus also used, as for $\text{PuO}_3(\text{g})$, the electronic spectrum of PuO_2^{2+} , but the main discrepancy in the standard entropy is due to the treatment of the vibrational frequencies. Actually, in Ebbinghaus' work a full analogy to $\text{UO}_2(\text{OH})_2(\text{g})$ was assumed, and the simulation treated the two torsional modes (for this molecule, internal rotations of OH groups) with the hindered rotor approach instead of harmonic oscillators. Nonetheless, in a recent study related to the thermodynamic properties of $\text{UO}_2(\text{OH})_2(\text{g})$ [82], no specific treatment has been made because it has been pointed out as an unreliable approach for these molecules in a previous review [83]. Therefore, similar behavior could be expected for $\text{PuO}_2(\text{OH})_2(\text{g})$ molecule: for reasons of computational cost, internal rotations are treated as other vibrations. Finally, for all these reasons, we prefer to rely on our calculations and we propose the following standard entropy of $\text{PuO}_2(\text{OH})_2(\text{g})$ at room temperature:

$$S_{298 \text{ K}}^\ominus = 355.74 \text{ J K}^{-1} \text{ mol}^{-1}, \quad (15)$$

which is lower by $22.1 \text{ J K}^{-1} \text{ mol}^{-1}$ than Ebbinghaus' data ($377.8 \text{ J K}^{-1} \text{ mol}^{-1}$). The heat capacity function (in $\text{J K}^{-1} \text{ mol}^{-1}$) is:

$$C_p^\ominus(T) = 119.4872 + 3.3686 \times 10^{-2}(T/K) - 9.5789 \times 10^{-6}(T/K)^2 - 1.6030 \times 10^6(T/K)^{-2} \quad (16)$$

in the 298.15–1000 K range, and

$$C_p^\ominus(T) = 134.27 + 1.5303 \times 10^{-2}(T/K) - 2.0559 \times 10^{-6}(T/K)^2 - 5.5254 \times 10^6(T/K)^{-2} \quad (17)$$

in the 1000–3000 K higher temperature range.

With respect to the standard heat of formation, the same drawbacks as for the PuO_3 molecule are pointed out regarding the experimental measurements carried out by Krikorian et al. [5]. Additional issues may increase the uncertainty in this case, as the authors had to do some estimates related to water weighting in order to measure the steam pressure in the apparatus [5]. Thus, our calculations, which are not completely off from the reported experimental estimation $(-1018.2 \pm 3.3) \text{ kJ mol}^{-1}$ [5], can be considered as the most reliable ones. Our best estimate (SO-CASPT2) for the standard heat of formation thus is

$$\Delta_f H^\ominus(298.15 \text{ K}) = (-1012.6 \pm 38.1) \text{ kJ mol}^{-1}. \quad (18)$$

Thermodynamic Equilibrium Calculations

From an experimental viewpoint, the existence of $\text{PuO}_3(\text{g})$ remains an open issue. The most recent analysis, involving mass spectrometric studies, performed on the plutonium vapor phase in the Pu+O system, has not detected the PuO_3^+ vaporous species in the apparatus, whatever the vacuum or oxidative environment [78]. However, the authors concluded that dedicated experiments are needed to state the existence of this vapor species especially due to the previous study by Ronchi where PuO_3 was briefly detected [4].

To investigate the chemical equilibrium of the vapor phase over the plutonium oxygen phase with the current thermodynamic data, thermodynamic equilibrium computations were performed within the Nuclea Toolbox software [87] and the self-consistent MEPHISTA (version 17_1) database designed for nuclear fuel [88]. Isochoric calculations in which the oxygen amount is varying (associated with constant plutonium quantity) are made to show the plutonium vapor trend versus the oxygen potential. The simulation was run at 2270 K to reproduce the experiment under oxidative conditions, carried out by Gotcu-Freis et al. [78]. Attention should be focused at the oxygen potential equal to about -130 kJ mol^{-1} , corresponding to the oxygen pressure of 100 Pa applied during the experiment. In order to perceive the effect of the newly determined thermodynamics functions, a first calculation with the original thermodynamic database (MEPHISTA-17_1) was performed (Figure 4a). At an oxygen potential of -130 kJ mol^{-1} the gaseous phase is mainly composed of PuO_2 though its partial pressure remains low. In addition, the contribution to the gaseous

TABLE IX: Standard Enthalpies of Formation ($\Delta_f H^\circ$ (298.15 K) in kJ mol^{-1}) of PuO_2 , $\text{PuO}_2(\text{OH})_2$, PuO_3 in the Gas Phase Calculated at Various Level of Theory and Extrapolated to the Complete Basis Set (CBS) limit and Obtained from the Average over the Six Teactions Listed in Table I, except for ${}^2\text{DC}^{\text{M}}\text{-CCSD(T)}$ for Which the Average only Includes Four Reactions R3–R6. ΔE_{SO} represents the spin-orbit contribution to the enthalpy, which is included in all SO-method results. The uncertainties $\Delta\Delta_f H^\circ$ correspond to 95% confidence intervals are computed with the formulas [84] given in the Supporting Information

Method	PuO_2	PuO_3	$\text{PuO}_2(\text{OH})_2$
ΔE_{SO}^a	34.4	59.0	46.9
SO-B3LYP ^b	-318.4 ± 20.6	-405.7 ± 22.5	-801.9 ± 30.3
SO-UCCSD	-353.3 ± 16.2	NC	NC
SO-UCCSD(T)	-411.2 ± 6.6	NC	NC
${}^2\text{DC}^{\text{M}}\text{-CCSD}^c$	-409.3 ± 14.9	NC	NC
${}^2\text{DC}^{\text{M}}\text{-CCSD(T)}^c$	-449.5 ± 8.8	NC	NC
SO-CASPT2	-413.7 ± 18.5	-553.2 ± 27.5	-1012.6 ± 38.1
Experiment	-410 ± 20 [85]; -428.7 ± 7.0 [78] -440 ± 7 [78]; -412 ± 20 [86] -428.7 ± 20.0 [2]	-562.8 ± 5.0 [5] -567.6 ± 15.0 [2]	-1018.2 ± 3.3 [5]

^a ΔE_{SO} is the estimate of the SO contribution; ^b The energies of reactions were estimated with a RECP and the associated basis set of triple ζ quality for the plutonium. Thus, no CBS was performed; ^c Uncertainties over four reactions R3–R6;

phase of PuO increases as the oxygen’s chemical potential decreases.

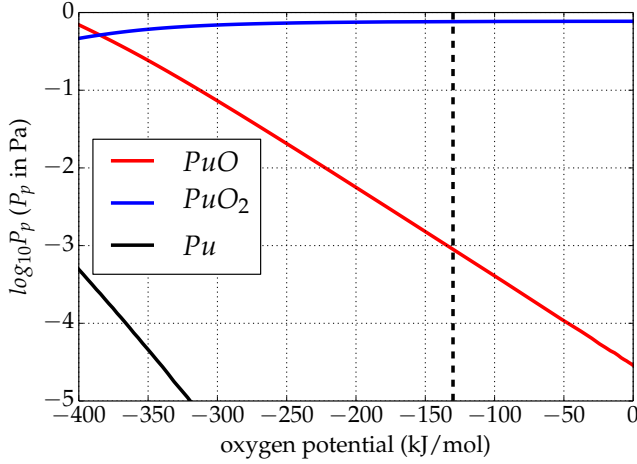
Conversely, with the updated database (Figure 4b), i.e. $\text{PuO}_3(\text{g})$ is added and the Gibbs function of $\text{PuO}_2(\text{g})$ is modified according to the present work. Unlike the first simulation, PuO_3 appears in the gaseous phase up to low oxygen potentials, whereas its partial pressure is higher than that of PuO for an oxygen potential of about -130 kJ mol^{-1} . This appears to contradict the analysis of Gotcu-Freis et al. [78], in which PuO is detected whereas the same is not true for PuO_3 . The dissociation energy of PuO_3 to PuO_2^+ is 1032 kJ mol^{-1} , calculated from the reviewed data of the ionization energy of PuO_2 (7.07 eV). The SO-CASPT2 calculations allow us to propose the value of 9.2 eV ($887.5 \text{ kJ mol}^{-1}$) for the adiabatic ionization energy for PuO_3 , about 0.9 eV lower than that predicted (10.1 eV) by scalar relativistic DFT calculations [89]. The PuO_3 ionization energy is just below the dissociation energy and therefore suggests that the fragmentation of PuO_3 to PuO_2^+ could be an important process and explains why PuO_3 is not detected. Finally, even if the temperature is high, these simulations show that the total partial pressure of plutonium remains rather low, whatever the database. At high oxygen potentials, a temperature drop should promote the plutonium trioxide over the dioxide with nevertheless a partial pressure lower than that obtained at 2270 K.

To extend the investigation to an oxygen/steam environment case, thermodynamic equilibrium calculations were also done under isobaric condition (standard pressure) with a constant amount of oxygen while a variable hydrogen inventory was used in order to shift the oxygen potential. The partial pressures of gaseous plutonium species versus the oxygen potential were calculated at the lowest possible temperature (1500 K) at which gaseous

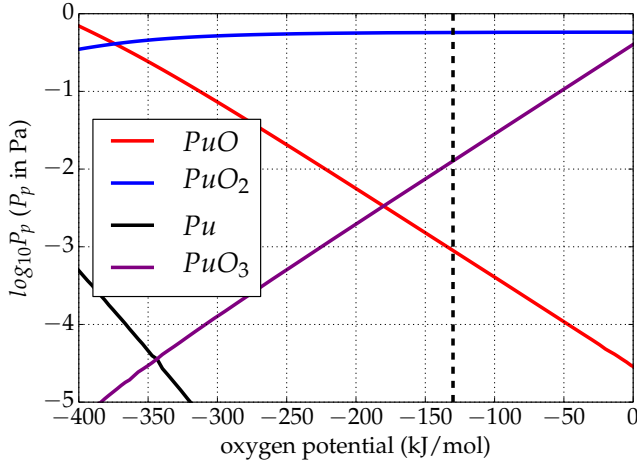
plutonium is present, and in accordance with the simulation temperature used in the experiments dedicated to Pu(VI) volatility performed by Krikorian et al. [5] and Hubener et al. [6]. At this temperature, the plutonium volatility is very low: i.e., $< 10^{-11}$ bar whatever the oxygen potential. Under a purely oxygen atmosphere, as expected, only PuO_3 appears, but if steam is present, the $\text{PuO}_2(\text{OH})_2$ species exists and rapidly becomes the main gaseous species when the steam fraction rises (see Fig. 5).

CONCLUSIONS

In conclusion, this work proposes a complete revision of the thermodynamics functions of the main gaseous species of the Pu–O–H system, namely PuO_2 , PuO_3 , and $\text{PuO}_2(\text{OH})_2$, using accurate relativistic correlated quantum chemical calculations extrapolated to the complete basis set limit. This updated database is helpful to predict the most important thermophysical properties for nuclear safety and risk analysis: namely, the vapor pressure. Thermodynamic equilibrium calculations with the updated database performed at high temperature disclose new aspects of the volatility of plutonium under accidental conditions. They not only confirm the predominance of PuO_2 under an oxygen atmosphere, but also validate the conjecture of Ronchi et al. [4] and Krikorian et al. [5] regarding the formation of the molecule $\text{PuO}_3(\text{g})$ at high oxygen potentials. However, all reported quantum chemical calculations suggest that the stability of $\text{PuO}_3(\text{g})$ might be hampered by fragmentation processes to lower-valent oxides. In the presence of steam, plutonium volatilizes into two competing Pu(VI) gaseous forms, $\text{PuO}_3(\text{g})$, and $\text{PuO}_2(\text{OH})_2(\text{g})$, though their par-



(a) MEPHISTA-17_1



(b) Modified database

FIG. 4: Thermodynamic equilibrium calculations : focus on the partial pressures of plutonium species at 2270 K versus the chemical potential of oxygen. The dashed line corresponds to an oxygen pressure of 100 Pa (-130 kJ mol^{-1}).

tial pressures are low: *i.e.*, $< 10^{-11}$ bar. This study increases the knowledge of the effective volatility of plutonium and calls for caution assessments and possibly new experiments in secured nuclear laboratories.

In addition to the nuclear implications, new insights into the electronic structure of the plutonium oxide and oxyhydroxide species have been gained, by confronting the results obtained with the two-component relativistic correlated $^2\text{DC}^{\text{M}}$ -CCSD method and the more approximate two-step relativistic multireference method SO-CASPT2. Our SO-CASPT2 and $^2\text{DC}^{\text{M}}$ -EOM-EE-CCSD results confirm the initial evidence by Feng and Peterson [42] that the ground state of PuO_2 is closed-shell at

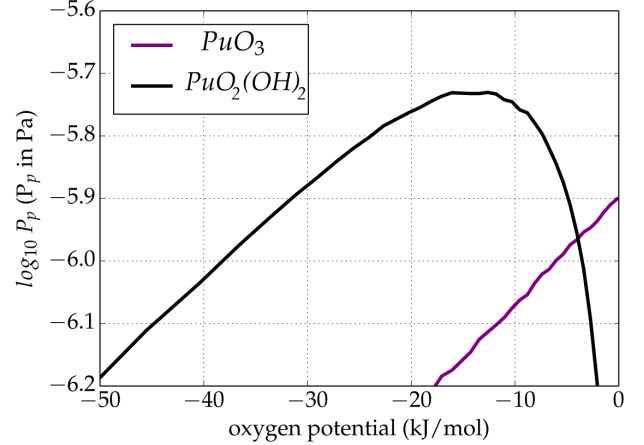


FIG. 5: Focus on the partial pressures of plutonium species at 1500 K versus the chemical potential of oxygen under standard pressure conditions for the Pu-O-H system.

the relativistic level with a $\Omega = 0_g^+$ character and provide compelling evidence that it is well separated by about several thousands of cm^{-1} from the first open-shell u-state formally assigned as the PuO_2 ground state by La Macchia et al. [51] $^2\text{DC}^{\text{M}}$ -EOM-IP-CCSD calculations place the adiabatic ionization energy of PuO_2 at 7.07 eV, in excellent agreement with the up-to-date experimental value. The electronic ground states of PuO_3 and $\text{PuO}_2(\text{OH})_2$ exhibit strong multireference characters, and we evidence that multi-reference SO-CASPT2 is a quantitatively appropriate method to compute their enthalpies of formation. The reported values are in good agreement with the available data, making us confident about its predictive capability for other gas-phase heavy element species with complex electronic structures.

ACKNOWLEDGEMENTS

We gratefully acknowledge financial support from the France-Canada Research Fund, Natural Sciences and Engineering Research Council of Canada (NSERC). This research was supported by the NEEDS environment project (TEMPO, “Thermodynamique des Molécules de Plutonium”) funded in 2017. We acknowledge support by the French government through the Program “Investissement d’avenir” (LABEX CaPPA / ANR-11-LABX-0005-01 and I-SITE ULNE / ANR-16-IDEX-0004 ULNE), as well as by the Ministry of Higher Education and Research, Hauts de France council and European Regional Development Fund (ERDF) through the Contrat de Projets Etat-Region (CPER CLIMIBIO). Furthermore, this work was granted access to the HPC resources of [CINES/IDRIS/TGCC] under the allocation 2016-

2019 [x2016081859 and A0010801859, A0030801859, A0050800244] made by GENCI. We also acknowledge Małgorzata Olejniczak for her exploratory work on the benchmarking of relativistic DFT and MS-CASPT2 calculations. We further thank Sidi Souvi and Marc Barachin for the very fruitful discussions.

ASSOCIATED CONTENT

The following file, ms-PuOx-ESI.pdf is available free of charge. It contains:

- Mathematical formula used to compute the uncertainties.
- Figure illustrating the ANO-RCC basis set convergence to the CBS limit.
- Analysis of the spin-free and spin-orbit states of Pu, PuO₂, PuO₃, and PuO₂(OH)₂ and their SO-CASPT2 transition energies, up to 16 000 cm⁻¹;
- Molecular parameters and standard entropies of the PuO₂(g), PuO₃(g), and PuO₂(OH)₂(g) molecules;
- The heat capacity functions of the PuO₂(g), PuO₃(g), and PuO₂(OH)₂(g) molecules.
- Atomization energies of PuO₂.

The full data set distributed through the Zenodo repository [90].

-
- * Department of Chemistry and Chemical Biology, McMaster University, 1280 Main Street West, Hamilton L8S 4M1, Canada
- [1] M. Šulka, L. Cantrel, and V. Vallet, *J. Phys. Chem. A* **118**, 10073 (2014).
 - [2] R. J. M. Konings, O. Beneš, A. Kovács, D. Manara, D. Sedmidubský, L. Gorokhov, V. S. Iorish, V. Yungman, E. Shenyavskaya, and E. Osina, *J. Phys. Chem. Ref. Data* **43**, 013101 (2014), <https://doi.org/10.1063/1.4825256>.
 - [3] C. Guéneau, C. Chatillon, and B. Sundman, *J. Nucl. Mater.* **378**, 257 (2008).
 - [4] C. Ronchi, F. Capone, J. Y. Colle, and J. P. Hiernaut, *J. Nucl. Mater.* **280**, 111 (2000).
 - [5] O. H. Krikorian, A. S. Fontes, B. B. Ebbinghaus, and M. G. Adamson, *J. Nucl. Mater.* **247**, 161 (1997).
 - [6] S. Hübener, S. Taut, A. Vahle, G. Bernhard, and T. Fanghänel, *Radiochim. Acta* **96**, 781 (2008).
 - [7] J. Sikkema, L. Visscher, T. Saue, and M. Iliáš, *J. Chem. Phys.* **131**, 124116 (2009).
 - [8] I. Infante, A. S. P. Gomes, and L. Visscher, *J. Chem. Phys.* **125**, 074301 (2006).
 - [9] I. Infante, E. Eliav, M. J. Vilkas, Y. Ishikawa, U. Kaldor, and L. Visscher, *J. Chem. Phys.* **127**, 124308 (2007).
 - [10] K. Boguslawski, F. Réal, P. Tecmer, C. Duperrouzel, A. S. P. Gomes, Ö. Legeza, P. W. Ayers, and V. Vallet, *Phys. Chem. Chem. Phys.* **19**, 4317 (2017), [arXiv:1608.02353 \[physics.chem-ph\]](https://arxiv.org/abs/1608.02353).
 - [11] A. Kovács, *J. Mol. Struct.* **1132**, 95 (2017).
 - [12] A. S. P. Gomes, C. R. Jacob, and L. Visscher, *Phys. Chem. Chem. Phys.* **10**, 5353 (2008).
 - [13] F. Ruipérez, C. Danilo, F. Réal, J.-P. Flament, V. Vallet, and U. Wahlgren, *J. Phys. Chem. A* **113**, 1420 (2009).
 - [14] A. Weigand, X. Cao, V. Vallet, J.-P. Flament, and M. Dolg, *J. Phys. Chem. A* **113**, 11509 (2009).
 - [15] F. Réal, A. S. P. Gomes, L. Visscher, V. Vallet, and E. Eliav, *J. Phys. Chem. A* **113**, 12504 (2009).
 - [16] P. Tecmer, A. S. P. Gomes, U. Ekström, and L. Visscher, *Phys. Chem. Chem. Phys.* **13**, 6249 (2011).
 - [17] P. Tecmer, H. van Lingen, A. S. P. Gomes, and L. Visscher, *J. Chem. Phys.* **137**, 084308 (2012).
 - [18] A. S. P. Gomes, C. R. Jacob, F. Réal, V. Vallet, and L. Visscher, *Phys. Chem. Chem. Phys.* **15**, 15153 (2013).
 - [19] A. Shee, T. Saue, L. Visscher, and A. S. P. Gomes, *J. Chem. Phys.* **147**, 174113 (2018).
 - [20] E. G. Rauh and R. J. Ackermann, *J. Chem. Phys.* **60**, 1396 (1974), <https://doi.org/10.1063/1.1681210>.
 - [21] E. G. Rauh and R. J. Ackermann, *J. Chem. Phys.* **64**, 1862 (1974), <https://doi.org/10.1063/1.432738>.
 - [22] F. Capone, Y. Colle, J. P. Hiernaut, and C. Ronchi, *J. Phys. Chem. A* **103**, 10899 (1999), <https://doi.org/10.1021/jp992405f>.
 - [23] M. Santos, J. Marçalo, A. Pires de Matos, J. K. Gibson, and R. G. Haire, *J. Phys. Chem. A* **106**, 7190 (2002), <https://doi.org/10.1021/jp025733f>.
 - [24] B. Ruscic and D. H. Bross, “Active thermochemical tables (atct) values based on ver. 1.122e of the thermochemical network, argonne national laboratory (2019); available at atct.anl.gov,” (2019).
 - [25] R. J. Lemire, J. Fuger, H. Nitsche, P. Potter, M. H. Rand, J. Rydberg, K. Spahiu, J. A. Sullivan, W. J. Ullman,

- P. Vitorge, and H. Wanner, *Chemical Thermodynamics of Neptunium and Plutonium*, edited by OECD Nuclear Energy Agency, Chemical thermodynamics (Elsevier, 2001).
- [26] W. K \ddot{u} chle, M. Dolg, H. Stoll, and H. Preuss, *J. Chem. Phys.* **100**, 7535 (1994).
- [27] X. Cao, M. Dolg, and H. Stoll, *J. Chem. Phys.* **118**, 487 (2003).
- [28] T. H. Dunning, Jr., *J. Chem. Phys.* **90**, 1007 (1989).
- [29] A. D. Becke, *J. Chem. Phys.* **98**, 5648 (1993).
- [30] M. J. Frisch, G. W. Trucks, H. B. Schlegel, G. E. Scuseria, M. A. Robb, J. R. Cheeseman, J. A. Montgomery, Jr., T. Vreven, K. N. Kudin, J. C. Burant, J. M. Millam, S. S. Iyengar, J. Tomasi, V. Barone, B. Mennucci, M. Cossi, G. Scalmani, N. Rega, G. A. Petersson, H. Nakatsuji, M. Hada, M. Ehara, K. Toyota, R. Fukuda, J. Hasegawa, M. Ishida, T. Nakajima, Y. Honda, O. Kitao, H. Nakai, M. Klene, X. Li, J. E. Knox, H. P. Hratchian, J. B. Cross, V. Bakken, C. Adamo, J. Jaramillo, R. Gomperts, R. E. Stratmann, O. Yazyev, A. J. Austin, R. Cammi, C. Pomelli, J. W. Ochterski, P. Y. Ayala, K. Morokuma, G. A. Voth, P. Salvador, J. J. Dannenberg, V. G. Zakrzewski, S. Dapprich, A. D. Daniels, M. C. Strain, O. Farkas, D. K. Malick, A. D. Rabuck, K. Raghavachari, J. B. Foresman, J. V. Ortiz, Q. Cui, A. G. Baboul, S. Clifford, J. Cioslowski, B. B. Stefanov, G. Liu, A. Liashenko, P. Piskorz, I. Komaromi, R. L. Martin, D. J. Fox, T. Keith, M. A. Al-Laham, C. Y. Peng, A. Nanayakkara, M. Challacombe, P. M. W. Gill, B. Johnson, W. Chen, M. W. Wong, C. Gonzalez, and J. A. Pople, "Gaussian 09, Revision C.02," Gaussian, Inc., Wallingford, CT, 2004.
- [31] V. Barone, *J. Chem. Phys.* **120**, 3059 (2004).
- [32] V. Barone, *J. Chem. Phys.* **122**, 014108 (2005).
- [33] B. O. Roos, R. Lindh, P.-Å. Malmqvist, V. Veryazov, and P.-O. Widmark, *J. Phys. Chem. A* **108**, 2851 (2004).
- [34] B. O. Roos, R. Lindh, P.-Å. Malmqvist, V. Veryazov, and P.-O. Widmark, *Chem. Phys. Lett.* **409**, 295 (2005).
- [35] A. Karton and J. M. L. Martin, *Theor. Chem. Acc.* **115**, 330 (2006).
- [36] D. Feller, K. A. Peterson, and D. A. Dixon, *J. Chem. Phys.* **129**, 204105 (2008).
- [37] D. Feller, K. A. Peterson, and J. Grant Hill, *J. Chem. Phys.* **135**, 044102 (2011).
- [38] Q. Lu and K. A. Peterson, *J. Chem. Phys.* **145**, 054111 (2016).
- [39] J. D. Watts, J. Gauss, and R. J. Bartlett, *J. Chem. Phys.* **98**, 8718 (1993).
- [40] H.-J. Werner, P. J. Knowles, G. Knizia, F. R. Manby, M. Schütz, P. Celani, W. Györffy, D. Kats, T. Korona, R. Lindh, A. Mitrushenkov, G. Rauhut, K. R. Shamasundar, T. B. Adler, R. D. Amos, A. Bernhardsson, A. Berning, D. L. Cooper, M. J. O. Deegan, A. J. Dobbyn, F. Eckert, E. Goll, C. Hampel, A. Hesselmann, G. Hetzer, T. Hrenar, G. Jasen, C. Köppl, Y. Liu, A. W. Lloyd, R. A. Mata, A. J. May, S. J. McNicholas, W. Meyer, M. E. Mura, A. Nicklass, D. P. O'Neill, P. Palmieri, D. Peng, K. Pflüger, R. Pitzer, M. Reiher, T. Shiozaki, H. Stoll, A. J. Stone, R. Tarroni, T. Thorsteinsson, and M. Wang, "Molpro, version 2015.1, a package of *Ab Initio* programs," (2015), see <http://www.molpro.net>.
- [41] D. H. Bross and K. A. Peterson, *J. Chem. Phys.* **141**, 244308 (2014).
- [42] R. Feng, M. Vasiliu, K. A. Peterson, and D. A. Dixon, *J. Phys. Chem. A* **121**, 1041 (2017).
- [43] L. Gagliardi and B. O. Roos, *Chem. Soc. Rev.* **36**, 893 (2007).
- [44] P. J. Knowles and H.-J. Werner, *Chem. Phys. Lett.* **115**, 259 (1985).
- [45] H.-J. Werner and P. J. Knowles, *J. Chem. Phys.* **82**, 5053 (1985).
- [46] L. Bovey and S. Gerstenkorn, *J. Opt. Soc. Am.* **51**, 522 (1961).
- [47] J. Blaise, M. Fred, S. Gerstenkorn, and B. Judd, *C.R. Acad. Sci., Fr.* **255**, 2403 (1962).
- [48] J. Blaise, J. F. Wyart, J. G. Conway, and E. F. Worden, *Phys. Scr.* **22**, 224 (1980).
- [49] P.-Å. Malmqvist, A. Rendell, and B. O. Roos, *J. Phys. Chem.* **94**, 5477 (1990).
- [50] R. G. Denning, *J. Phys. Chem. A* **111**, 4125 (2007).
- [51] G. La Macchia, I. Infante, J. Raab, J. K. Gibson, and L. Gagliardi, *Phys. Chem. Chem. Phys.* **10**, 7278 (2008).
- [52] J. Stårling, A. Bernhardsson, and R. Lindh, *Molecular Physics, Mol. Phys.* **99**, 103 (2001).
- [53] J. Finley, P.-Å. Malmqvist, B. O. Roos, and L. Serrano-Andrés, *Chem. Phys. Lett.* **288**, 299 (1998).
- [54] N. Forsberg and P.-Å. Malmqvist, *Chem. Phys. Lett.* **274**, 196 (1997).
- [55] G. Ghigo, B. O. Roos, and P.-Å. Malmqvist, *Chem. Phys. Lett.* **396**, 142 (2004).
- [56] P.-Å. Malmqvist, B. O. Roos, and B. Schimmelpfennig, *Chem. Phys. Lett.* **357**, 230 (2002).
- [57] B. A. Heß, C. M. Marian, U. Wahlgren, and O. Gropen, *Chem. Phys. Lett.* **251**, 365 (1996).
- [58] B. Schimmelpfennig, "Amfi, an atomic mean-field integral program," (1996).
- [59] A. Francesco, A. Jochen, C. R. K., C. L. F., D. M. G., D. V. Luca, F. G. Ignacio, F. Nicolas, F. L. Manuel, G. Laura, G. Marco, G. Angelo, H. C. E., L. M. Giovanni, L. Hans, M. Dongxia, M. P. Åke, M. Thomas, N. Artur, O. Massimo, P. T. Bondo, P. Daoling, P. Felix, P. Ben, R. Markus, R. Ivan, S. Igor, S. Javier, S. Michael, T. D. G., U. Liviu, V. Alessio, V. Steven, V. Valera, V. V. P., W. Oliver, Z. Felipe, and L. Roland, *J. Comput. Chem.* **37**, 506 (2015).
- [60] L. Visscher, T. J. Lee, and K. G. Dyall, *J. Chem. Phys.* **105**, 8769 (1996).
- [61] L. Visscher, E. Eliav, and U. Kaldor, *J. Chem. Phys.* **115**, 9720 (2001).
- [62] DIRAC, a relativistic ab initio electronic structure program, Release DIRAC18 (2018), written by T. Saue, L. Visscher, H. J. Aa. Jensen, and R. Bast, with contributions from V. Bakken, K. G. Dyall, S. Dubillard, U. Ekström, E. Eliav, T. Enevoldsen, E. Faßhauer, T. Fleig, O. Fossgaard, A. S. P. Gomes, E. D. Hedegård, T. Helgaker, J. Henriksson, M. Iliaš, Ch. R. Jacob, S. Knecht, S. Komorovský, O. Kullie, J. K. Lærdahl, C. V. Larsen, Y. S. Lee, H. S. Nataraj, M. K. Nayak, P. Norman, G. Olejniczak, J. Olsen, J. M. H. Olsen, Y. C. Park, J. K. Pedersen, M. Pernpointner, R. di Remigio, K. Ruud, P. Salek, B. Schimmelpfennig, A. Shee, J. Sikkema, A. J. Thorvaldsen, J. Thyssen, J. van Stralen, S. Villaume, O. Visser, T. Winther, and S. Yamamoto (available at <https://doi.org/10.5281/zenodo.2253986>, see also <http://www.diracprogram.org>).
- [63] K. G. Dyall, *Theor. Chem. Acc.* **131**, 1172 (2012).
- [64] K. G. Dyall, *Theor. Chem. Acc.* **117**, 491 (2007).

- [65] L. Visscher, *Theor. Chem. Acc.* **98**, 68 (1997).
- [66] J. Thyssen, *Development and Applications of Methods for Correlated Relativistic Calculations of Molecular Properties*, Ph.D. thesis, University of Southern Denmark (2001).
- [67] A. Kovács, *J. Phys. Chem. A* **121**, 2523 (2017).
- [68] R. Feng and K. A. Peterson, *J. Chem. Phys.* **147**, 084108 (2017).
- [69] I. Infante, A. Kovacs, G. La Macchia, A. R. Moughal Shahi, J. K. Gibson, and L. Gagliardi, *J. Phys. Chem. A* **114**, 6007 (2010).
- [70] E. F. Archibong and A. K. Ray, *J. Mol. Struct.: THEOCHEM* **530**, 165 (2000).
- [71] E. R. Batista, R. L. Martin, P. J. Hay, J. E. Peralta, and G. E. Scuseria, *J. Chem. Phys.* **121**, 2144 (2004).
- [72] F. Capone, J. Y. Colle, J. P. Hiernaut, and C. Ronchi, *J. Phys. Chem. A* **109**, 12054 (2005).
- [73] J. K. Gibson, M. Santos, J. Marçalo, J. P. Leal, A. Pires de Matos, and R. G. Haire, *J. Phys. Chem. A* **110**, 4131 (2006).
- [74] B. B. Ebbinghaus, *Calculated thermodynamic functions for gas phase uranium, neptunium, plutonium and americium oxides (AnO_3), oxyhydroxides ($AnO_2(OH)_2$), oxychlorides (AnO_2Cl_2) and oxyfluorides (AnO_2F_2)*, Tech. Rep. UCRL-ID-122278 (Lawrence Livermore National Laboratory, CA (US), 2002).
- [75] D. W. Green and G. T. Reedy, *J. Chem. Phys.* **69**, 544 (1978).
- [76] A. Kovács, R. J. M. Konings, J. K. Gibson, I. Infante, and L. Gagliardi, *Chemical Reviews*, *Chem. Rev.* **115**, 1725 (2015).
- [77] F. Miradji, S. Souvi, L. Cantrel, F. Louis, and V. Vallet, *J. Phys. Chem. A* **119**, 4961 (2015).
- [78] P. Gotcu-Freis, J.-Y. Colle, J.-P. Hiernaut, F. Naisse, C. Guéneau, and R. J. M. Konings, *J. Chem. Thermodyn.* **43**, 1164 (2011).
- [79] J. C. Eisenstein and M. H. L. Pryce, *J. Res. Natl. Bur. Stand., Sect. A* **70A**, 165 (1966).
- [80] O. H. Krikorian, B. B. Ebbinghaus, M. G. Adamson, A. S. Fontes, Jr., and D. L. Fleming, *Experimental Studies and Thermodynamic Modeling of Volatilities of Uranium, Plutonium, and Americium from Their Oxides and from Their Oxides Interacted with Ash*, Report UCRL-ID-114774 (Lawrence Livermore National Laboratory, CA (United States), 1993).
- [81] The uncertainties are given within a level of confidence of 95 percent.
- [82] R. J. M. Konings, A. Kovács, and O. Beneš, *J. Nucl. Mater.* **496**, 163 (2017).
- [83] R. Guillaumont, T. Fanghänel, V. Neck, J. Fuger, D. A. Palmer, I. Grenthe, and M. H. Rand, *Update on the chemical thermodynamics of uranium, neptunium, plutonium, americium and technetium*, Tech. Rep. (OECD Nuclear Energy Agency, OECD Nuclear Energy Agency, Data Bank Issy-les-Moulineaux, France, 2003).
- [84] B. Ruscic, J. E. Boggs, A. Burcat, A. G. Császár, J. Demaison, R. Janoschek, J. M. L. Martin, M. L. Morton, M. J. Rossi, J. F. Stanton, and et al., *J. Phys. Chem. Ref. Data* **34**, 573 (2005).
- [85] E. H. P. Cordfunke and R. J. M. Konings, *J. Phase Equilib.* **14**, 457 (1993).
- [86] V. Glushko, L. Gurvich, I. Veits, V. Medvedev, G. Khachkuruzov, V. Yungman, and G. Bergman, *Thermodynamic Properties of Individual Substances*, edited by V. G. (Ed.), Vol. 1-4 (Nauka, Moscow, 1978-1982).
- [87] B. Piar, “Nucleatoolbox 2.3.0,” IRSN.
- [88] B. Cheynet and E. Fischer, unpublished (2007).
- [89] T. Gao, Z.-H. Zhu, X.-L. Wang, Y. Sun, and D.-Q. Meng, *Chin. J. Chem.* **62**, 454 (2004).
- [90] S. Kervazo, F. Réal, F. Viot, A. S. P. Gomes, and V. Vallet, “Accurate predictions of volatile plutonium thermodynamic properties,” Zenodo <http://dx.doi.org/10.5281/zenodo.3380352> (2019).

Supporting information for: Accurate Predictions of Volatile Plutonium Thermodynamic Properties

Sophie Kervazo,[†] Florent Réal,[†] François Viot,[¶] André Severo Pereira Gomes,[†]
and Valérie Vallet^{*,†}

[†]*Université de Lille, CNRS, UMR 8523 – PhLAM – Physique des Lasers, Atomes et
Molécules, F-59000 Lille*

[‡]*Department of Chemistry and Chemical Biology, McMaster University, Hamilton, 1280
Main Street West, L8S 4M1, Canada*

[¶]*Institut de Radioprotection et de Sécurité Nucléaire (IRSN), PSN-RES, Cadarache, St Paul
Lez Durance 13115, France*

E-mail: valerie.vallet@univ-lille.fr

Contents

List of Tables

- S1 Standard enthalpies of formation of the molecules in kJ mol^{-1} taken from the Active Thermochemical Tables^{S1} and from Ref.^{S2} for Pu; Zero-Point Vibrational energy and enthalpy increment $H^\ominus(298.15\text{ K})-H^\ominus(0\text{ K})$ computed at the B3LYP level with aug-cc-pVTZ basis sets. S10
- S2 Fine structure transition energies (ΔE in cm^{-1}) of atomic Pu computed at the SO-CASPT2 level with the ANO-RCC-TZVP basis set, and analysis of the various J -states in terms of the dominating LS terms. S11
- S3 Vertical transition energies (ΔE in cm^{-1} , up to $16\,000\text{ cm}^{-1}$) of PuO_3 at the SF-CASPT2 and SO-CASPT2 levels obtained with the ANO-RCC-TZVP. Weights of the reference wavefunction in the CASPT2 perturbation treatment are given for the SF states. Orbitals $1a_1$, $2a_1/\pi_u$, $3a_1$ being always doubly occupied, they do not appear in the following table. S12
- S4 Vertical transition energies (ΔE in cm^{-1} , up to $16\,000\text{ cm}^{-1}$) of $\text{PuO}_2(\text{OH})_2$ at the SF-CASPT2 and SO-CASPT2 levels obtained with the ANO-RCC-TZVP basis sets. Weights of the reference wavefunction in the CASPT2 perturbation treatment are given for the SF states. S18
- S5 Vertical transition energies (ΔE in cm^{-1} , up to $16\,000\text{ cm}^{-1}$) of PuO_2 ((Distance Pu–O = 1.808 \AA) at SF-CASPT2 and SO-CASPT2 levels obtained with the ANO-RCC-TZVP basis sets. Weights of the reference wavefunction in the CASPT2 perturbation treatment are given for the SF states. The $1a_g$, $1b_{1u}/\sigma_u$ and $1b_{3u}/2p$ orbitals being always doubly occupied, they do not appear in the table. S21
- S6 Number of electronic states at MS-CASPT2 level of calculations. S27

S7	The molecular parameters of $\text{PuO}_2(\text{g})$ obtained at the CBS $^2\text{DC}^{\text{M}}\text{-CCSD}(\text{T})$ level. All electronic states (and their degeneracy in brackets) are not written here, but any levels listed in Table 6 (CBS- $^2\text{DC}^{\text{M}}\text{-EOM-CCSD}$ values) are taken into account in the calculation of thermodynamic functions.	S27
S8	The molecular parameters of $\text{PuO}_3(\text{g})$. Electronic states are not degenerate, all levels are not written here, but any states listed in Table S3 are taken into account in the calculation of thermodynamic functions.	S28
S9	The molecular parameters of $\text{PuO}_2(\text{OH})_2(\text{g})$. Electronic states are not degenerate, all levels are not written here, but any states listed in Table S4 are taken into account in the calculation of thermodynamic functions.	S28
S10	Standard entropies at 298.15 K (in $\text{J K}^{-1} \text{mol}^{-1}$) with detailed contributions. ^a Moments of inertia have been calculated from geometries got in Ref. S3 within Gaussian09 package. ^b Two internal rotations have been treated by author with hindered rotor instead harmonic oscillator.	S28
S11	0 K atomization energies (AE_0 , in kJ mol^{-1}) of PuO_2 , corresponding to the opposite of Reaction R2 at various levels of theory	S29
S12	Summary of contributions to the composite calculation of the reaction enthalpies leading to PuO_2 in kJ mol^{-1} , and derived standard enthalpy of formation with its uncertainty. The final average values includes all reactions, except for the $^2\text{DC}^{\text{M}}\text{-CCSD}$ and $^2\text{DC}^{\text{M}}\text{-CCSD}(\text{T})$ values which are averaged over reactions R ₃ –R ₆	S30
S13	Summary of contributions to the composite calculation of the reaction enthalpies leading to PuO_3 in kJ mol^{-1} , and derived standard enthalpy of formation with its uncertainty. The final average values includes all reactions.	S32
S14	Summary of contributions to the composite calculation of the reaction enthalpies leading to $\text{PuO}_2(\text{OH})_2$ in kJ mol^{-1} , and derived standard enthalpy of formation with its uncertainty. The final average values includes all reactions.	S33

List of Figures

S1	ANO-RCC basis set convergence to the CBS limit (taken as 0) of the reaction energies at 0 K for the reactions R ₁ –R ₆ leading to the formation of PuO ₂ (a), PuO ₃ (b) and PuO ₂ (OH) ₂ (c).	S9
S2	Heat capacity of PuO ₂ (g). Konings' assessment refers to Ref. S4	S34
S3	Heat capacity of PuO ₃ (g). Konings' assessment refers to Ref. S4 and Ebbinghaus' data to Ref. S3	S35
S4	Heat capacity of PuO ₂ (OH) ₂ (g). Ebbinghaus' data refers to Ref. S3	S35

Details on uncertainties evaluations

To comply with the standards of the Active Thermochemical Tables developed by Ruscic, all standard enthalpies of formation reported in the paper are associated with uncertainties corresponding to the 95% confidence intervals.

The uncertainties of the derived enthalpies of formation from a given chemical reaction are derived from the formula:

$$2\sigma_m = \left[\sum_i (2\nu_i\sigma_i)^2 \right]^{1/2} \quad (1)$$

$2\sigma_i$ are the uncertainties of the standard enthalpies of formation of the species entering the chemical reaction, and ν_i are the reaction stoichiometric coefficients.

The final standard enthalpies of formation are obtained from a weighted average μ of the n values x_i , ($i = 1, \dots, n$), where each values have an associated uncertainty σ_i , $i = 1, \dots, n$, and are obtained from the expression:^{S5}

$$\mu = \frac{\sum_{i=1}^n (x_i/\sigma_i^2)}{\sum_{i=1}^n (1/\sigma_i^2)} \quad (2)$$

The variance s_μ of μ is then

$$s_\mu = \left(\frac{\sum_{i=1}^n [(x_i - \mu)^2/\sigma_i^2]}{(n-1) \sum_{i=1}^n 1/\sigma_i^2} \right)^{1/2} \quad (3)$$

To bring the final uncertainty closer to the 95% confidence limits, s_μ is multiplied by a factor of 2.^{S5}

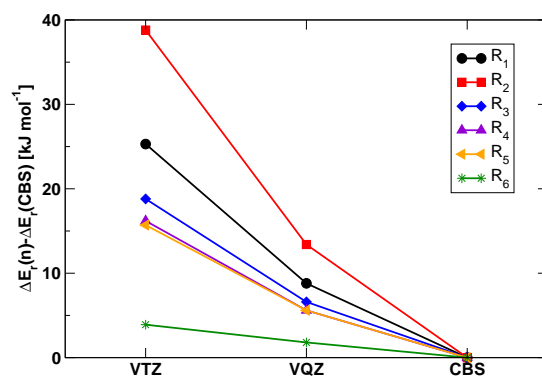
In our case, the largest uncertainty to the standard enthalpies of formation associated to the available literature data regarding each reaction is that of the plutonium atom with a

value of $\pm 3 \text{ kJ mol}^{-1}$ (see Table S1). All the reactions have the same inherited uncertainty, thus have the same weight in the calculated weighted average of Eq. 2. Thus, to also account for the uncertainty of σ_{Pu} , the total uncertainty s_{μ}^{tot} (reported in Tables S12, S13, S14) associated to the average over all the considered reaction is calculated as:

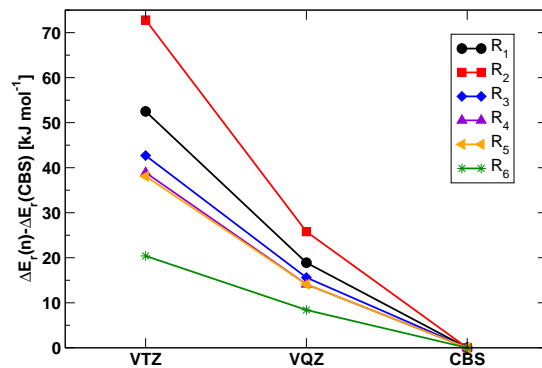
$$s_{\mu}^{\text{tot}} = \sqrt{(2s_{\mu})^2 + (2\sigma_{\text{Pu}})^2} \quad (4)$$

Basis set convergence to the basis set limit

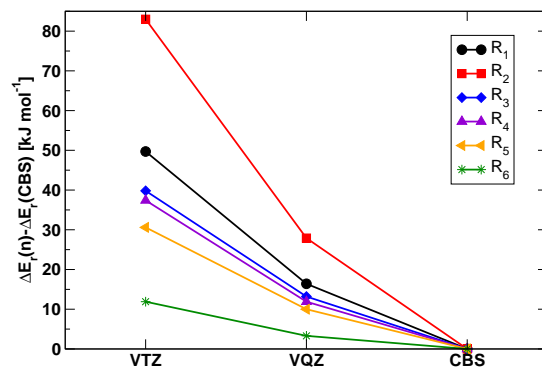
All energies have been extrapolated to the complete basis set limit, using Equations (4) and (5) of the article. For lanthanide complexes, Lu and Peterson^{S6} reported irregular convergence pattern of the ANO-RCC basis sets. However, for Pu complexes, the convergence is smooth, as illustrated by Figure S1.



(a) PuO₂



(b) PuO₃



(c) PuO₂(OH)₂

Figure S1: ANO-RCC basis set convergence to the CBS limit (taken as 0) of the reaction energies at 0 K for the reactions R₁–R₆ leading to the formation of PuO₂ (a), PuO₃ (b) and PuO₂(OH)₂ (c).

Table S1: Standard enthalpies of formation of the molecules in kJ mol^{-1} taken from the Active Thermochemical Tables^{S1} and from Ref. S2 for Pu; Zero-Point Vibrational energy and enthalpy increment $H^\ominus(298.15\text{ K})-H^\ominus(0\text{ K})$ computed at the B3LYP level with aug-cc-pVTZ basis sets.

Species	$\Delta_f H^\ominus(298.15\text{ K})$	ZPE	$H^\ominus(298.15\text{ K})-H^\ominus(0\text{ K})$
O (3P)	249.2290 \pm 0.0021	0	6.73
H (1S)	217.998 \pm 0.000	0	6.20
Pu (5F)	349.00 \pm 3.00	0	6.20
H ₂	0.0	26.44	8.68
H ₂ O	-241.835 \pm 0.027	53.10	9.93
H ₂ O ₂	-135.464 \pm 0.063	69.33	10.96
O ₂	0.0	9.72	8.68
OH	37.489 \pm 0.027	22.08	8.68
PuO ₂		11.50	12.35
PuO ₃		16.32	15.34
PuO ₂ (OH) ₂		80.47	21.33
PuO ₂ ⁺		14.68	11.41
PuO ₃ ⁺		18.07	14.73

Table S2: Fine structure transition energies (ΔE in cm^{-1}) of atomic Pu computed at the SO-CASPT2 level with the ANO-RCC-TZVP basis set, and analysis of the various J -states in terms of the dominating LS terms.

J -value	ΔE	Weight of LS states
0	0	54% 7F , 38% 5D , 7% 3P
1	1806	64% 7F , 32% 5D
2	4208	82% 7F , 17% 5D
3	6353	88% 7F , 10% 5D
4	8091	93% 7F
5	9552	90% 7F
6	11 010	85% 7F , 10% 5G
0	12 499	44% 7F , 21% 5D , 8% 3P
1	13 612	66% 9H , 9% 7F , 7% 7G
2	14 399	82% 9H , 14% 7G
1	14 845	38% 5D , 20% 7F , 9% 9G
3	15 551	89% 9H , 8% 7G
4	17 026	86% 9H , 6% 7G
1	17 032	66% 9D , 29% 7P

Table S3: Vertical transition energies (ΔE in cm^{-1} , up to $16\,000\text{cm}^{-1}$) of PuO_3 at the SF-CASPT2 and SO-CASPT2 levels obtained with the ANO-RCC-TZVP. Weights of the reference wavefunction in the CASPT2 perturbation treatment are given for the SF states. Orbitals $1a_1$, $2a_1/\pi_u$, $3a_1$ being always doubly occupied, they do not appear in the following table.

State	Character : % [orbital(number of electron)]	ΔE	Ref. weight
SF-CASPT2 states			
(1) ³ B ₂	36% [4a ₁ /p ^(O) (2), 1b ₁ /φ _u (1), 1b ₂ /p ^(O) ($\bar{1}$), 2b ₂ /σ _u (2), 3b ₂ /δ _u (1), 1a ₂ /δ _u (1)] 21% [4a ₁ /p ^(O) (2), 1b ₁ /φ _u (1), 1b ₂ /p ^(O) (1), 2b ₂ /σ _u (2), 3b ₂ /δ _u ($\bar{1}$), 1a ₂ /δ _u (1)] 22% [4a ₁ /p ^(O) (2), 1b ₁ /φ _u (1), 1b ₂ /p ^(O) (2), 2b ₂ /σ _u (2), 1a ₂ /δ _u (1)]	0	0.72
(1) ³ A ₂	43% [4a ₁ /p ^(O) (2), 5a ₁ /φ _u (1), 1b ₂ /p ^(O) ($\bar{1}$), 2b ₂ /σ _u (2), 3b ₂ /δ _u (1), 1a ₂ /δ _u (1)] 23% [4a ₁ /p ^(O) (2), 5a ₁ /φ _u (1), 1b ₂ /p ^(O) (1), 2b ₂ /σ _u (2), 3b ₂ /δ _u ($\bar{1}$), 1a ₂ /δ _u (1)] 17% [4a ₁ /p ^(O) (2), 5a ₁ /φ _u (1), 1b ₂ /p ^(O) (2), 2b ₂ /σ _u (2), 1a ₂ /δ _u (1)]	3161	0.72
(1) ³ B ₁	38% [4a ₁ /p ^(O) (2), 5a ₁ /φ _u (1), 1b ₁ /φ _u (1), 1b ₂ /p ^(O) ($\bar{1}$), 2b ₂ /σ _u (2), 3b ₂ /δ _u (1)] 12% [4a ₁ /p ^(O) (2), 5a ₁ /φ _u (1), 2b ₁ /π _u (1), 1b ₂ /p ^(O) ($\bar{1}$), 2b ₂ /σ _u (2), 3b ₂ /δ _u (1)] 12% [4a ₁ /p ^(O) (2), 5a ₁ /φ _u (1), 1b ₁ /φ _u (1), 2b ₁ /π _u (2), 1b ₂ /p ^(O) (2)]	4663	0.72
(1) ¹ A ₁	32% [4a ₁ /p ^(O) (2), 1b ₂ /p ^(O) (1), 2b ₂ /σ _u (2), 3b ₂ /δ _u ($\bar{1}$), 1a ₂ /δ _u (2)] 28% [4a ₁ /p ^(O) (2), 1b ₂ /p ^(O) (2), 2b ₂ /σ _u (2), 1a ₂ /δ _u (2)] 11% [4a ₁ /p ^(O) (1), 5a ₁ /φ _u ($\bar{1}$), 1b ₂ /p ^(O) (2), 2b ₂ /σ _u (2), 1a ₂ /δ _u (2)]	7239	0.70
(2) ³ A ₂	20% [4a ₁ /p ^(O) (2), 1b ₁ /φ _u (1), 1b ₂ /p ^(O) (1), 2b ₂ /σ _u (2), 3b ₂ /δ _u (2)] 18% [4a ₁ /p ^(O) (1), 5a ₁ /φ _u ($\bar{1}$), 1b ₁ /φ _u (1), 1b ₂ /p ^(O) (2), 2b ₂ /σ _u (2), 3b ₂ /δ _u (1)] 17% [4a ₁ /p ^(O) (2), 1b ₁ /φ _u (1), 1b ₂ /p ^(O) (2), 2b ₂ /σ _u (2), 3b ₂ /δ _u (1)]	7287	0.70
(2) ³ B ₁	31% [4a ₁ /p ^(O) (1), 5a ₁ /φ _u ($\bar{1}$), 1b ₂ /p ^(O) (2), 2b ₂ /σ _u (2), 3b ₂ /δ _u (1), 1a ₂ /δ _u (1)] 11% [4a ₁ /p ^(O) (2), 5a ₁ /φ _u (1), 2b ₁ /π _u (1), 1b ₂ /p ^(O) ($\bar{1}$), 2b ₂ /σ _u (2), 3b ₂ /δ _u (1)] 10% [4a ₁ /p ^(O) (2), 1b ₂ /p ^(O) (2), 2b ₂ /σ _u (2), 3b ₂ /δ _u (1), 1a ₂ /δ _u (1)] 10% [4a ₁ /p ^(O) (2), 1b ₁ /φ _u (1), 2b ₁ /π _u (1), 1b ₂ /p ^(O) ($\bar{1}$), 2b ₂ /σ _u (2), 1a ₂ /δ _u (1)]	8038	0.70
(1) ⁵ B ₂	47% [4a ₁ /p ^(O) (2), 1b ₁ /φ _u ($\bar{1}$)(1), 1b ₂ /p ^(O) (2), 2b ₂ /σ _u (1), 3b ₂ /δ _u (1), 1a ₂ /δ _u (1)] 41% [4a ₁ /p ^(O) (2), 5a ₁ /φ _u (1), 1b ₁ /φ _u ($\bar{1}$)(1), 1b ₂ /p ^(O) (1), 2b ₂ /σ _u (2), 1a ₂ /δ _u (1)]	8962	0.73
(1) ³ A ₁	39% [4a ₁ /p ^(O) (2), 1b ₁ /φ _u ($\bar{1}$)(1), 2b ₁ /π _u (1), 1b ₂ /p ^(O) ($\bar{1}$), 2b ₂ /σ _u (2), 3b ₂ /δ _u (1)] 11% [4(2), 1b ₁ /φ _u ($\bar{1}$)(1), 8(1), 1b ₂ /p ^(O) ($\bar{1}$), 2b ₂ /σ _u (2), 3b ₂ /δ _u (1)]	9645	0.72
(2) ³ B ₂	15% [4a ₁ /p ^(O) (2), 2b ₁ /π _u (1), 1b ₂ /p ^(O) (2), 2b ₂ /σ _u (2), 1a ₂ /δ _u (1)]	9731	0.70

Table S3 – Continued from previous page

State	Character : % [orbital(number of electron)]	ΔE	Ref. weight
(1) ¹ A ₂	15% [4a ₁ /p ^(O) (1), 5a ₁ /φ _u ($\bar{1}$), 2b ₁ /π _u (1), 1b ₂ /p ^(O) (2), 2b ₂ /σ _u (2), 1a ₂ /δ _u (1)]	10 293	0.72
	12% [4a ₁ /p ^(O) (2), 2b ₁ /π _u (1), 1b ₂ /p ^(O) ($\bar{1}$), 2b ₂ /σ _u (2), 3b ₂ /δ _u (1), 1a ₂ /δ _u (1)]		
	26% [4a ₁ /p ^(O) (2), 5a ₁ /φ _u (1), 1b ₂ /p ^(O) (1), 2b ₂ /σ _u (2), 11($\bar{1}$), 1a ₂ /δ _u ($\bar{1}$)]		
	24% [4a ₁ /p ^(O) (2), 5a ₁ /φ _u (1), 1b ₂ /p ^(O) ($\bar{1}$), 2b ₂ /σ _u (2), 3b ₂ /δ _u (1), 1a ₂ /δ _u ($\bar{1}$)]		
	18% [4a ₁ /p ^(O) (2), 1b ₁ /φ _u (1), 1b ₂ /p ^(O) ($\bar{1}$), 2b ₂ /σ _u (2), 1a ₂ /δ _u (2)]		
	16% [4a ₁ /p ^(O) (2), 5a ₁ /φ _u (1), 1b ₂ /p ^(O) (2), 2b ₂ /σ _u (2), 1a ₂ /δ _u ($\bar{1}$)]		
(1) ¹ B ₂	30% [4a ₁ /p ^(O) (2), 1b ₁ /φ _u (1), 1b ₂ /p ^(O) ($\bar{1}$), 2b ₂ /σ _u (2), 3b ₂ /δ _u (1), 1a ₂ /δ _u ($\bar{1}$)]	10 604	0.72
	22% [4a ₁ /p ^(O) (2), 1b ₁ /φ _u (1), 1b ₂ /p ^(O) (1), 2b ₂ /σ _u (2), 3b ₂ /δ _u ($\bar{1}$), 1a ₂ /δ _u ($\bar{1}$)]		
	16% [4a ₁ /p ^(O) (2), 1b ₁ /φ _u (1), 1b ₂ /p ^(O) (2), 2b ₂ /σ _u (2), 1a ₂ /δ _u ($\bar{1}$)]		
	15% [4a ₁ /p ^(O) (2), 5a ₁ /φ _u (1), 1b ₂ /p ^(O) ($\bar{1}$), 2b ₂ /σ _u (2), 1a ₂ /δ _u (2)]		
(1) ⁵ A ₁	27% [4a ₁ /p ^(O) (2), 5a ₁ /φ _u (1), 1b ₁ /φ _u (1), 1b ₂ /p ^(O) (2), 2b ₂ /σ _u (1), 1a ₂ /δ _u (1)]	10 662	0.72
	15% [4a ₁ /p ^(O) (2), 2b ₁ /π _u [*] (1), 1b ₁ /φ _u (1), 1b ₂ /p ^(O) (2), 2b ₂ /σ _u (1), 1a ₂ /δ _u (1)]		
	12% [4a ₁ /p ^(O) (2), 5a ₁ /φ _u (1), 1b ₁ /φ _u (1), 1b ₂ /p ^(O) (1), 2b ₂ /σ _u (2), 1a ₂ /δ _u (1)]		
(3) ³ B ₁	26% [4a ₁ /p ^(O) (2), 1b ₁ /φ _u (1), 2b ₁ /π _u (1), 1b ₂ /p ^(O) ($\bar{1}$), 2b ₂ /σ _u (2), 1a ₂ /δ _u (1)]	11 567	0.71
	17% [4a ₁ /p ^(O) (1), 5a ₁ /φ _u ($\bar{1}$), 1b ₂ /p ^(O) (2), 2b ₂ /σ _u (2), 3b ₂ /δ _u (1), 1a ₂ /δ _u (1)]		
(1) ¹ B ₁	34% [4a ₁ /p ^(O) (2), 1b ₂ /p ^(O) (1), 2b ₂ /σ _u (2), 3b ₂ /δ _u (2), 1a ₂ /δ _u ($\bar{1}$)]	11 632	0.1
	18% [4a ₁ /p ^(O) (1), 5a ₁ /φ _u ($\bar{1}$), 1b ₂ /p ^(O) (2), 2b ₂ /σ _u (2), 3b ₂ /δ _u (1), 1a ₂ /δ _u ($\bar{1}$)]		
	17% [4a ₁ /p ^(O) (2), 1b ₂ /p ^(O) (2), 2b ₂ /σ _u (2), 3b ₂ /δ _u (1), 1a ₂ /δ _u ($\bar{1}$)]		
(1) ⁵ B ₁	36% [4a ₁ /p ^(O) (2), 1b ₁ /φ _u (1), 2b ₁ /π _u (1), 1b ₂ /p ^(O) (2), 2b ₂ /σ _u (1), 1a ₂ /δ _u (1)]	12 017	0.72
	15% [4a ₁ /p ^(O) (2), 1b ₁ /φ _u (1), 2b ₁ /π _u (1), 1b ₂ /p ^(O) (1), 2b ₂ /σ _u (2), 1a ₂ /δ _u (1)]		
(1) ⁵ A ₂	36% [4a ₁ /p ^(O) (2), 1b ₁ /φ _u (1), 2b ₁ /π _u (1), 1b ₂ /p ^(O) (2), 2b ₂ /σ _u (1), 1a ₂ /δ _u (1)]	12 017	0.72
	15% [4a ₁ /p ^(O) (2), 1b ₁ /φ _u (1), 2b ₁ /π _u (1), 1b ₂ /p ^(O) (1), 2b ₂ /σ _u (2), 1a ₂ /δ _u (1)]		
(3) ³ B ₂	24% [4a ₁ /p ^(O) (2), 1b ₁ /φ _u (1), 1b ₂ /p ^(O) (1), 2b ₂ /σ _u (2), 3b ₂ /δ _u (1), 1a ₂ /δ _u ($\bar{1}$)]	12 023	0.72
	11% [4a ₁ /p ^(O) (2), 5a ₁ /φ _u (1), 1b ₂ /p ^(O) (1), 2b ₂ /σ _u (2), 3b ₂ /δ _u (2)]		
(3) ³ A ₂	17% [4a ₁ /p ^(O) (2), 1b ₁ /φ _u (1), 1b ₂ /p ^(O) (1), 2b ₂ /σ _u (2), 1a ₂ /δ _u (2)]	12 940	0.71
	15% [4a ₁ /p ^(O) (2), 5a ₁ /φ _u (1), 1b ₂ /p ^(O) (1), 2b ₂ /σ _u (2), 3b ₂ /δ _u (1), 1a ₂ /δ _u ($\bar{1}$)]		
(2) ¹ A ₁	21% [4a ₁ /p ^(O) (2), 5a ₁ /φ _u (2), 1b ₂ /p ^(O) (1), 2b ₂ /σ _u (2), 3b ₂ /δ _u ($\bar{1}$)]	13 213	0.70
	10% [4a ₁ /p ^(O) (1), 5a ₁ /φ _u ($\bar{1}$), 1b ₂ /p ^(O) (2), 2b ₂ /σ _u (2), 3b ₂ /δ _u (2)]		
	10% [4a ₁ /p ^(O) (2), 5a ₁ /φ _u (2), 1b ₂ /p ^(O) (2), 2b ₂ /σ _u (2)]		
(2) ³ A ₁	44% [4a ₁ /p ^(O) (2), 5a ₁ /φ _u (1), 1b ₁ /φ _u (1), 1b ₂ /p ^(O) ($\bar{1}$), 2b ₂ /σ _u (2), 1a ₂ /δ _u (1)]	13 421	0.73

Table S3 – Continued from previous page

State	Character : % [orbital(number of electron)]	ΔE	Ref. weight
(4) ³ B ₁	29% [4a ₁ /p ^(O) (2), 5a ₁ /φ _u (1), 2b ₁ /π _u (1), 1b ₂ /p ^(O) ($\bar{1}$), 2b ₂ /σ _u (2), 1a ₂ /δ _u (1)]	13 518	0.71
	29% [4a ₁ /p ^(O) (2), 2b ₁ /π _u [*] (1), 1b ₁ /φ _u (1), 1b ₂ /p ^(O) ($\bar{1}$), 2b ₂ /σ _u (2), 3b ₂ /δ _u (1)]		
	15% [4a ₁ /p ^(O) (2), 5a ₁ /φ _u (1), 2b ₁ /π _u (1), 1b ₂ /p ^(O) ($\bar{1}$), 2b ₂ /σ _u (2), 3b ₂ /δ _u (1)]		
	13% [4a ₁ /p ^(O) (2), 2b ₁ /π _u [*] (1), 1b ₁ /φ _u (1), 1b ₂ /p ^(O) (2), 2b ₂ /σ _u (2)]		
(2) ⁵ A ₁	11% [4a ₁ /p ^(O) (2), 5a ₁ /φ _u (1), 2b ₁ /π _u [*] (1), 1b ₂ /p ^(O) ($\bar{1}$), 2b ₂ /σ _u (2), 1a ₂ /δ _u (1)]	13 575	0.72
	29% [4a ₁ /p ^(O) (2), 1b ₁ /φ _u (1), 2b ₁ /π _u (1), 1b ₂ /p ^(O) (2), 2b ₂ /σ _u (1), 3b ₂ /δ _u (1)]		
	14% [4a ₁ /p ^(O) (2), 5a ₁ /φ _u (1), 1b ₁ /φ _u (1), 1b ₂ /p ^(O) (2), 2b ₂ /σ _u (1), 1a ₂ /δ _u (1)]		
	13% [4a ₁ /p ^(O) (2), 1b ₁ /φ _u (1), 2b ₁ /π _u (1), 1b ₂ /p ^(O) (1), 2b ₂ /σ _u (2), 3b ₂ /δ _u (1)]		
(2) ⁵ B ₁	12% [4a ₁ /p ^(O) (2), 5a ₁ /φ _u (1), 2b ₁ /π _u (1), 1b ₂ /p ^(O) (2), 2b ₂ /σ _u (1), 1a ₂ /δ _u (1)]	13 970	0.73
	30% [4a ₁ /p ^(O) (2), 5a ₁ /φ _u (1), 1b ₁ /φ _u (1), 1b ₂ /p ^(O) (2), 2b ₂ /σ _u (1), 3b ₂ /δ _u (1)]		
	20% [4a ₁ /p ^(O) (2), 5a ₁ /φ _u (1), 1b ₁ /φ _u (1), 1b ₂ /p ^(O) (1), 2b ₂ /σ _u (2), 3b ₂ /δ _u (1)]		
	16% [4a ₁ /p ^(O) (2), 5a ₁ /φ _u (1), 2b ₁ /π _u (1), 1b ₂ /p ^(O) (2), 2b ₂ /σ _u (1), 3b ₂ /δ _u (1)]		
(2) ⁵ A ₂	10 % [4a ₁ /p ^(O) (2), 5a ₁ /φ _u (1), 2b ₁ /π _u (1), 1b ₂ /p ^(O) (1), 2b ₂ /σ _u (2), 3b ₂ /δ _u (1)]	13 971	0.73
	30% [4a ₁ /p ^(O) (2), 5a ₁ /φ _u (1), 1b ₁ /φ _u (1), 1b ₂ /p ^(O) (2), 2b ₂ /σ _u (1), 3b ₂ /δ _u (1)]		
	20% [4a ₁ /p ^(O) (2), 5a ₁ /φ _u (1), 1b ₁ /φ _u (1), 1b ₂ /p ^(O) (1), 2b ₂ /σ _u (2), 3b ₂ /δ _u (1)]		
	16% [4a ₁ /p ^(O) (2), 5a ₁ /φ _u (1), 2b ₁ /π _u (1), 1b ₂ /p ^(O) (2), 2b ₂ /σ _u (1), 3b ₂ /δ _u (1)]		
(3) ⁵ B ₁	10% [4a ₁ /p ^(O) (2), 5a ₁ /φ _u (1), 2b ₁ /π _u (1), 1b ₂ /p ^(O) (1), 2b ₂ /σ _u (2), 3b ₂ /δ _u (1)]	14 055	0.73
	86% [4a ₁ /p ^(O) (1), 5a ₁ /φ _u (1), 1b ₂ /p ^(O) (2), 2b ₂ /σ _u (2), 3b ₂ /δ _u (1), 1a ₂ /δ _u (1)]		
(3) ⁵ A ₂	86% [4a ₁ /p ^(O) (1), 5a ₁ /φ _u (1), 1b ₂ /p ^(O) (2), 2b ₂ /σ _u (2), 3b ₂ /δ _u (1), 1a ₂ /δ _u (1)]	14 056	0.73
(3) ⁵ A ₁	80% [4a ₁ /p ^(O) (1), 1b ₁ /φ _u (1), 1b ₂ /p ^(O) (2), 2b ₂ /σ _u (2), 3b ₂ /δ _u (1), 1a ₂ /δ _u (1)]	14 139	0.72
(3) ³ A ₁	58% [4a ₁ /p ^(O) (1), 1b ₁ /φ _u ($\bar{1}$), 1b ₂ /p ^(O) (2), 2b ₂ /σ _u (2), 3b ₂ /δ _u (1), 1a ₂ /δ _u (1)]	14 236	0.73
	20% [4a ₁ /p ^(O) (1), 1b ₁ /φ _u (1), 1b ₂ /p ^(O) (2), 2b ₂ /σ _u (2), 3b ₂ /δ _u ($\bar{1}$), 1a ₂ /δ _u (1)]		
	10% [4a ₁ /p ^(O) (1), 1b ₁ /φ _u (1), 1b ₂ /p ^(O) (2), 2b ₂ /σ _u (2), 3b ₂ /δ _u (1), 1a ₂ /δ _u ($\bar{1}$)]		
(4) ³ B ₂	19% [4a ₁ /p ^(O) (1), 5a ₁ /φ _u ($\bar{1}$), 1b ₁ /φ _u (1), 1b ₂ /p ^(O) (2), 2b ₂ /σ _u (2), 1a ₂ /δ _u (1)]	14 843	0.71
	18% [4a ₁ /p ^(O) (2), 5a ₁ /φ _u (1), 1b ₂ /p ^(O) (1), 2b ₂ /σ _u (2), 3b ₂ /δ _u (2)]		
(3) ¹ A ₁	27% [4a ₁ /p ^(O) (2), 1b ₁ /φ _u (2), 1b ₂ /p ^(O) (1), 2b ₂ /σ _u (2), 3b ₂ /δ _u ($\bar{1}$)]	14 889	0.71
	13% [4a ₁ /p ^(O) (2), 1b ₁ /φ _u (2), 1b ₂ /p ^(O) (2), 2b ₂ /σ _u (2)]		
(2) ¹ A ₂	47% [4a ₁ /p ^(O) (2), 1b ₁ /φ _u (1), 1b ₂ /p ^(O) ($\bar{1}$), 2b ₂ /σ _u (2), 3b ₂ /δ _u (2)]	14 984	0.72
	10% [4a ₁ /p ^(O) (2), 5a ₁ /φ _u (1), 1b ₂ /p ^(O) ($\bar{1}$), 2b ₂ /σ _u (2), 3b ₂ /δ _u (1), 1a ₂ /δ _u ($\bar{1}$)]		
	9% [4a ₁ /p ^(O) (2), 5a ₁ /φ _u (1), 1b ₂ /p ^(O) (1), 2b ₂ /σ _u (2), 3b ₂ /δ _u ($\bar{1}$), 1a ₂ /δ _u ($\bar{1}$)]		

Table S3 – Continued from previous page

State	Character : % [orbital(number of electron)]	ΔE	Ref. weight
(2) ⁵ B ₂	64% [4a ₁ /p ^(O) (1), 5a ₁ /φ _u (1), 1b ₁ /φ _u (1), 1b ₂ /p ^(O) (2), 2b ₂ /σ _u (2), 1a ₂ /δ _u (1)] 10% [4a ₁ /p ^(O) (1), 6(1), 1b ₁ /φ _u (1), 1b ₂ /p ^(O) (2), 2b ₂ /σ _u (2), 1a ₂ /δ _u (1)]	15 035	0.72
(2) ¹ B ₁	33% [4a ₁ /p ^(O) (2), 5a ₁ /φ _u (1), 1b ₁ /φ _u ($\bar{1}$), 1b ₂ /p ^(O) (1), 2b ₂ /σ _u (2), 3b ₂ /δ _u ($\bar{1}$)] 13% [4a ₁ /p ^(O) (2), 5a ₁ /φ _u (1), 1b ₁ /φ _u ($\bar{1}$), 1b ₂ /p ^(O) (2), 2b ₂ /σ _u (2),] 12% [4a ₁ /p ^(O) (2), 1b ₂ /p ^(O) (1), 2b ₂ /σ _u (2), 3b ₂ /δ _u (2), 1a ₂ /δ _u ($\bar{1}$)] 11% [4a ₁ /p ^(O) (2), 5a ₁ /φ _u (2), 1b ₂ /p ^(O) (1), 2b ₂ /σ _u (2), 1a ₂ /δ _u ($\bar{1}$)]	15 593	0.72
SO-CASPT2 states			
X	47% (1) ³ B ₂ , 24% (1) ³ A ₂ , 14% (1) ³ B ₁		0
a	59% (1) ³ B ₂ , 25% (1) ³ A ₂		1235
b	74% (1) ³ B ₂		1783
c	51% (1) ³ A ₂		3777
d	24% (1) ³ B ₁ , 18% (1) ¹ A ₁ , 17% (2) ³ A ₂ , 10% (2) ³ B ₁		5660
e	49% (1) ³ B ₁ , 22% (1) ³ A ₁		6658
f	44% (1) ³ B ₁ , 19% (1) ³ A ₁ , 11% (2) ³ B ₁		7062
g	23% (1) ³ B ₂ , 18% (1) ³ A ₂ , 17% (2) ³ B ₁		7929
h	26% (1) ³ A ₂ , 21% (1) ⁵ B ₂ , 19% (2) ³ A ₂		7973
i	32% (2) ³ A ₂ , 24% (1) ³ A ₂ , 15% (1) ⁵ B ₂		8675
j	28% (1) ³ A ₂ , 22% (1) ³ B ₁ , 11% (1) ⁵ B ₂		9096
k	28% (1) ³ A ₂ , 26% (1) ³ B ₂		9345
l	31% (2) ³ B ₁ , 19% (1) ³ B ₁		9399
m	17% (1) ³ B ₂ , 15% (1) ⁵ B ₂		9690
n	29% (2) ³ B ₁ , 12% (2) ³ A ₁ , 10% (1) ³ B ₁		9879
o	24% (2) ³ A ₂ , 16% (1) ⁵ B ₁ , 13% (2) ³ B ₂		10 224
p	25% (2) ³ A ₂ , 15% (2) ³ B ₂ , 10% (1) ⁵ B ₁		10 235
q	23% (1) ⁵ B ₂ , 13% (3) ⁵ B ₁		10 342
r	29% (1) ⁵ B ₁ , 25% (1) ⁵ A ₁ , 10% (1) ⁵ B ₂ , 10% (2) ⁵ A ₁		10 686
s	23% (2) ³ B ₂ , 21% (3) ³ B ₁ , 15% (2) ³ B ₁		10 749
t	26% (1) ⁵ B ₁ , 21% (1) ⁵ A ₁ , 15% (1) ⁵ B ₂		10 768
u	24% (1) ⁵ B ₂ , 12% (3) ³ B ₁ , 10% (1) ⁵ A ₁		11 022

Table S3 – Continued from previous page

State	Character : % [orbital(number of electron)]	ΔE	Ref. weight
v	25% (1) ⁵ B ₂ , 21% (1) ⁵ A ₁ , 12% (1) ³ B ₁	11 207	
w	14% (1) ³ A ₁ , 10% (2) ³ A ₁	11 616	
x	36% (1) ⁵ A ₁ , 12% (2) ³ B ₁	12 429	
y	21% (2) ³ A ₂	12 567	
z	12% (1) ¹ A ₁ , 10% (3) ³ B ₁ , 10% (3) ³ B ₂	12 693	
aa	14% (1) ¹ A ₂	12 794	
ab	29% (2) ³ B ₂ , 24% (3) ³ A ₂	12 873	
ac	16% (3) ³ A ₁ , 15% (2) ⁵ B ₁ , 15% (1) ³ A ₁ , 11% (1) ⁵ B ₁	13 058	
ad	30% (3) ³ A ₂ , 14% (1) ¹ A ₁ ,	13 309	
ae	20% (2) ⁵ B ₁ , 13% (3) ⁵ A ₁ , 10% (2) ⁵ B ₂	13 341	
af	34% (3) ³ B ₂ , 17% (1) ¹ A ₂ , 12% (2) ¹ A ₂	13 488	
ag	25% (1) ³ A ₁ , 12% (2) ⁵ B ₁ , 11% (1) ⁵ B ₁	13 582	
ah	18% (2) ⁵ B ₁ , 15% (3) ⁵ A ₁	13 814	
ai	27% (1) ⁵ B ₂ , 15% (1) ¹ B ₂ , 12% (1) ³ A ₁	13 936	
aj	28% (1) ⁵ B ₂ , 19% (1) ⁵ A ₁ , 10% (2) ⁵ B ₁	13 996	
ak	18% (2) ⁵ B ₁ , 14% (3) ⁵ B ₁ , 12% (2) ⁵ A ₁ , 11% (1) ⁵ A ₁	14 024	
al	53% (1) ¹ B ₁ , 12% (3) ³ A ₂	14 216	
am	23% (2) ⁵ A ₁ , 13% (3) ⁵ B ₁ , 11% (3) ³ B ₁	14 257	
an	32% (1) ⁵ B ₂ , 10% (2) ³ A ₁	14 680	
ao	19% (1) ⁵ B ₁ , 17% (2) ⁵ B ₁ , 17% (3) ⁵ A ₁	14 724	
ap	21% (1) ⁵ A ₁ , 10% (2) ⁵ A ₁ , 10% (3) ⁵ B ₁	14 750	
aq	17% (3) ⁵ B ₁ , 13% (2) ⁵ B ₁ , 10% (2) ⁵ A ₁	14 874	
ar	16% (1) ⁵ B ₁	15 129	
as	20% (2) ⁵ A ₁ , 20% (1) ⁵ B ₁ , 13% (3) ⁵ B ₁ , 11% (3) ³ B ₁ , 10% (1) ⁵ A ₁	15 141	
at	29% (2) ³ B ₂ , 13% (1) ⁵ B ₂	15 375	
au	16% (2) ³ A ₁ , 12% (3) ⁵ B ₁ , 11% (1) ⁵ B ₁ , 10% (2) ³ B ₂	15 439	
av	26% (3) ³ B ₂ , 11% (2) ³ B ₂ , 10% (2) ⁵ A ₁	15 494	
aw	24% (3) ⁵ B ₁ , 12% (2) ³ A ₁ , 11% (3) ³ B ₁	15 616	
ay	13% (3) ⁵ A ₁ , 12% (2) ³ B ₁ , 11% (3) ³ A ₁ , 10% (3) ³ A ₂	15 708	
az	15% (3) ⁵ B ₁ , 11% (3) ³ B ₁	15 906	

Table S3 – *Continued from previous page*

State	Character : % [orbital(number of electron)]	ΔE	Ref. weight
ba	19% (3) ³ B ₂ , 17% (3) ⁵ B ₁	15 948	

Table S4: Vertical transition energies (ΔE in cm^{-1} , up to $16\,000\text{cm}^{-1}$) of $\text{PuO}_2(\text{OH})_2$ at the SF-CASPT2 and SO-CASPT2 levels obtained with the ANO-RCC-TZVP basis sets. Weights of the reference wavefunction in the CASPT2 perturbation treatment are given for the SF states.

State	Character : % [orbital(number of electron)]	ΔE	Ref. weight
SF-CASPT2 states			
(1) ³ B	49% 2a/ $\phi_u(1)$, 1b/ $\delta_u(1)$ 48% 1a/ $\delta_u(1)$, 2b/ $\phi_u(1)$	0	0.67
(1) ³ A	41% 1a/ $\delta_u(1)$, 2a/ $\phi_u(1)$ 59% 1b/ $\delta_u(1)$, 2b/ $\phi_u(1)$	889	0.67
(2) ³ B	75% 1a/ $\delta_u(1)$, 1b/ $\delta_u(1)$ 20% 2a/ $\phi_u(1)$, 2b/ $\phi_u(1)$	2136	0.67
(2) ³ A	59% 1a/ $\delta_u(1)$, 2a/ $\phi_u(1)$ 41% 1b/ $\delta_u(1)$, 2b/ $\phi_u(1)$	4698	0.67
(3) ³ B	52% 2a/ $\phi_u(1)$, 1b/ $\delta_u(1)$ 46% 1a/ $\delta_u(1)$, 2b/ $\phi_u(1)$	5351	0.67
(1) ¹ A	58% 1b/ $\delta_u(1)$, 2b/ $\phi_u(\bar{1})$ 30% 1a/ $\delta_u(1)$, 2a/ $\phi_u(\bar{1})$ 5% 2a/ $\phi_u(2)$	5764	0.66
(1) ¹ B	50% 1a/ $\delta_u(1)$, 1b/ $\delta_u(\bar{1})$ 28% 2a/ $\phi_u(1)$, 2b/ $\phi_u(\bar{1})$ 16% 1a/ $\delta_u(1)$, 2b/ $\phi_u(\bar{1})$	7444	0.66
(2) ¹ A	39% 1a/ $\delta_u(1)$, 2a/ $\phi_u(\bar{1})$ 29 % 2a/ $\phi_u(2)$ 13% 1b/ $\delta_u(1)$, 2b/ $\phi_u(\bar{1})$ 10% 1a/ $\delta_u(2)$	9626	0.66

Table S4 – Continued from previous page

State	Character : % [orbital(number of electron)]	ΔE	Ref. weight
	7 % 2a/ $\phi_u(2)$		
(3) ¹ A	44% 1b/ $\delta_u(2)$	10 184	0.66
	33% 2a/ $\phi_u(2)$		
	12% 2b/ $\phi_u(2)$		
	9% 1a/ $\delta_u(2)$		
(2) ¹ B	66% 2a/ $\phi_u(1)$, 2b/ $\phi_u(\bar{1})$	10 287	0.66
	26% 1a/ $\delta_u(1)$, 2b/ $\phi_u(\bar{1})$		
	8% 1a/ $\delta_u(1)$, 1b/ $\delta_u(\bar{1})$		
SO-CASPT2 states			
X	46% (1) ³ A, 41% (1) ³ B, 6% (2) ³ B	0	
a	45% (1) ³ B, 44% (1) ³ A, 6% (2) ³ B	323	
b	34% (2) ³ B, 25% (1) ³ B, 14% (1) ¹ A, 13% (2) ³ A, 10% (3) ³ B	2222	
c	40% (2) ³ A, 25% (2) ³ B, 19% ¹ B(1), 7% (1) ³ B, 6% (1) ³ A	3757	
d	36% (3) ³ B, 34% (2) ³ B, 14% (2) ¹ A, 11% (1) ³ B,	4158	
e	64% (1) ³ B, 30% (2) ³ B	7268	
f	93% (1) ³ A	7575	
g	32% (1) ¹ A, 28% (3) ³ B, 28% (2) ³ A, 6% (2) ³ B,	10 041	
h	41% (2) ³ A, 24% (3) ³ B, 15% (2) ³ B, 11% (1) ³ B, 6% ¹ B(1)	10 142	
i	34% (2) ³ A, 26% (2) ³ B, 14% (3) ³ B, 13% ¹ B(1), 8% (1) ³ B	10 343	
j	29% (2) ³ B, 26% (3) ³ B, 22% (1) ³ B, 17% (2) ¹ A	11 089	
k	26% (3) ³ B, 23% (1) ³ A, 17% (1) ³ B, 17% (2) ³ A, 13% (2) ³ B	12 269	
l	26% (2) ³ A, 24% (1) ³ A, 21% (3) ³ B, 15% (2) ³ B, 10% (1) ³ B	12 311	
m	28% (3) ³ B, 25% (2) ³ A, 22% (1) ³ A, 12% (1) ³ B, 10% (2) ³ B	13 782	
n	35% (3) ³ B, 22% (2) ³ A, 18% (1) ³ A, 13% (1) ³ B, 9% (2) ³ B	13 783	

Table S4 – *Continued from previous page*

State	Character : % [orbital(number of electron)]	ΔE	Ref. weight
o	41% (1) ¹ A, 20% (3) ¹ A, 15% (2) ³ B, 7% (4) ³ B,	15 696	

Table S5: Vertical transition energies (ΔE in cm^{-1} , up to $16\,000\text{ cm}^{-1}$) of PuO_2 (Distance $\text{Pu-O} = 1.808\text{ \AA}$) at SF-CASPT2 and SO-CASPT2 levels obtained with the ANO-RCC-TZVP basis sets. Weights of the reference wavefunction in the CASPT2 perturbation treatment are given for the SF states. The $1a_g$, $1b_{1u}/\sigma_u$ and $1b_{3u}/2p$ orbitals being always doubly occupied, they do not appear in the table.

State	Character : % [orbital(number of electron)]	ΔE	Ref. weight
SF-CASPT2 states			
(1) ⁵ A _g	84% [$1a_u/\delta_u(1)$, $2b_{2u}/\Phi_u(1)$, $2b_{1u}/\delta_u(1)$, $2b_{3u}/\Phi_u(1)$]	0	0.78
(2) ⁵ A _g	45% [$1a_u/\delta_u(1)$, $3b_{2u}/\pi_u(1)$, $2b_{1u}/\delta_u(1)$, $2b_{3u}/\Phi_u(1)$] 45% [$1a_u/\delta_u(1)$, $2b_{2u}/\Phi_u(1)$, $2b_{1u}/\delta_u(3)$, $3b_{3u}/\pi_u(1)$]	4798	0.78
(1) ⁵ B _{3u}	85% [$3a_g(1)$, $1a_u/\delta_u(1)$, $2b_{1u}/\delta_u(1)$, $2b_{3u}/\Phi_u(1)$]	5421	0.78
(1) ⁵ B _{2u}	85% [$3a_g(1)$, $1a_u/\delta_u(1)$, $2b_{1u}/\delta_u(1)$, $2b_{3u}/\Phi_u(1)$]	5421	
(1) ⁵ B _{3g}	44% [$2b_{2u}/\Phi_u(1)$, $3b_{2u}/\pi_u(1)$, $2b_{1u}/\delta_u(1)$, $2b_{3u}/\Phi_u(1)$] 44% [$1a_u/\delta_u(1)$, $2b_{2u}/\Phi_u(1)$, $2b_{3u}/\Phi_u(1)$, $3b_{3u}/\pi_u(1)$]	6019	0.78
(1) ⁵ B _{2g}	44% [$2b_{2u}/\Phi_u(1)$, $3b_{2u}/\pi_u(1)$, $2b_{1u}/\delta_u(1)$, $2b_{3u}/\Phi_u(1)$] 44% [$1a_u/\delta_u(1)$, $2b_{2u}/\Phi_u(1)$, $2b_{3u}/\Phi_u(1)$, $3b_{3u}/\pi_u(1)$]	6019	0.78
(3) ⁵ A _g	45% [$1a_u/\delta_u(1)$, $3b_{2u}/\pi_u(1)$, $2b_{1u}/\delta_u(1)$, $2b_{3u}/\Phi_u(1)$] 45% [$1a_u/\delta_u(1)$, $2b_{2u}/\Phi_u(1)$, $2b_{1u}/\delta_u(1)$, $3b_{3u}/\pi_u(1)$]	6067	0.78
(1) ⁵ B _{1g}	44% [$1a_u/\delta_u(1)$, $2b_{2u}/\Phi_u(1)$, $3b_{2u}/\pi_u(1)$, $2b_{1u}/\delta_u(1)$] 44% [$1a_u/\delta_u(1)$, $2b_{1u}/\delta_u(1)$, $2b_{3u}/\Phi_u(1)$, $3b_{3u}/\pi_u(1)$]	6158	0.78
(1) ³ B _{3u}	59% [$3a_g(1)$, $1a_u/\delta_u(\bar{1})$, $2b_{2u}/\Phi_u(1)$, $2b_{1u}/\delta_u(1)$] 19% [$3a_g(1)$, $1a_u/\delta_u(1)$, $2b_{2u}/\Phi_u(\bar{1})$, $2b_{1u}/\delta_u(1)$] 10% [$3a_g(1)$, $1a_u/\delta_u(1)$, $2b_{2u}/\Phi_u(1)$, $2b_{1u}/\delta_u(\bar{1})$]	6855	0.78
(1) ³ B _{2u}	59% [$3a_g(1)$, $1a_u/\delta_u(\bar{1})$, $2b_{1u}/\delta_u(1)$, $2b_{3u}/\Phi_u(1)$] 20% [$3a_g(1)$, $1a_u/\delta_u(1)$, $2b_{1u}/\delta_u(\bar{1})$, $2b_{3u}/\Phi_u(1)$]	6855	0.78
(2) ⁵ B _{1g}	44% [$1a_u/\delta_u(1)$, $2b_{1u}/\delta_u(1)$, $2b_{3u}/\Phi_u(1)$, $3b_{3u}/\pi_u(1)$] 44% [$1a_u/\delta_u(1)$, $2b_{2u}/\Phi_u(1)$, $3b_{2u}/\pi_u(1)$, $2b_{1u}/\delta_u(1)$]	7293	0.77
(1) ⁵ A _u	79% [$3a_g(1)$, $2b_{2u}/\Phi_u(1)$, $2b_{1u}/\delta_u(1)$, $2b_{3u}/\Phi_u(1)$]	7452	0.78
(1) ⁵ B _{1u}	80% [$3a_g(1)$, $1a_u/\delta_u(1)$, $2b_{2u}/\Phi_u(0)$, $2b_{3u}/\Phi_u(1)$]	7462	
(2) ⁵ B _{3g}	37% [$1a_u/\delta_u(1)$, $2b_{2u}/\Phi_u(1)$, $2b_{3u}/\Phi_u(1)$, $3b_{3u}/\pi_u(1)$] 33% [$2b_{2u}/\Phi_u(1)$, $3b_{2u}/\pi_u(1)$, $2b_{1u}/\delta_u(3)$, $2b_{3u}/\Phi_u(1)$] 12% [$2b_{2u}/\Phi_u(1)$, $3b_{2u}/\pi_u(1)$, $2b_{1u}/\delta_u(1)$, $3b_{3u}/\pi_u(1)$]	7637	0.78

Table S5 – Continued from previous page

State	Character : % [orbital(number of electron)]	ΔE	Ref. weight
(2) ⁵ B _{2g}	37% [1a _u /δ _u (1), 2b _{2u} /Φ _u (1), 2b _{3u} /Φ _u (1), 3b _{3u} /π _u (1)] 33% [2b _{2u} /Φ _u (1), 3b _{2u} /π _u (1), 2b _{1u} /δ _u (1), 2b _{3u} /Φ _u (1)] 12% [2b _{2u} /Φ _u (1), 3b _{2u} /π _u (1), 2b _{1u} /δ _u (1), 3b _{3u} /π _u (1)]	7637	0.78
(1) ³ B _{1u}	51% [3a _g (1), 1a _u /δ _u (1), 2b _{2u} /Φ _u ($\bar{1}$), 2b _{3u} /Φ _u (1)] 68% [3a _g (1), 1a _u /δ _u (1), 2b _{2u} /Φ _u ($\bar{1}$), 2b _{3u} /Φ _u (1)]	9586	0.78
(1) ³ A _u	51% [3a _g (1), 2b _{2u} /Φ _u ($\bar{1}$), 2b _{1u} /δ _u (1), 2b _{3u} /Φ _u (1)] 17% [3a _g (1), 2b _{2u} /Φ _u (1), 2b _{1u} /δ _u ($\bar{1}$), 2b _{3u} /Φ _u (1)]	9614	0.78
(1) ³ B _{3g}	38% [1a _u /δ _u (1), 2b _{2u} /Φ _u (1), 2b _{1u} /δ _u (2)] 36% [1a _u /δ _u (2), 2b _{1u} /δ _u (1), 2b _{3u} /Φ _u (1)]	10 101	0.79
(1) ³ B _{2g}	38% [1a _u /δ _u (1), 2b _{2u} /Φ _u (1), 2b _{1u} /δ _u (2)] 36% [1a _u /δ _u (2), 2b _{1u} /δ _u (1), 2b _{3u} /Φ _u (1)]	10 101	0.79
(1) ³ B _{1g}	24% [1a _u /δ _u (1), 2b _{2u} /Φ _u (2), 2b _{1u} /δ _u (1)] 24% [1a _u /δ _u (1), 2b _{1u} /δ _u (1), 2b _{3u} /Φ _u (2)] 19% [2b _{2u} /Φ _u (1), 2b _{1u} /δ _u (2), 2b _{3u} /Φ _u (1)] 16% [1a _u /δ _u (1), 2b _{2u} /Φ _u (1), 2b _{3u} /Φ _u (1)]	10 308	0.78
(2) ⁵ A _u	23% [3a _g (1), 1a _u /δ _u (1), 2b _{2u} /Φ _u (1), 3b _{2u} /π _u (1)] 23% [3a _g (1), 1a _u /δ _u (1), 2b _{3u} /Φ _u (1), 3b _{3u} /π _u (1)] 20% [3a _g (1), 3b _{2u} /π _u (1), 2b _{1u} /δ _u (1), 2b _{3u} /Φ _u (1)] 20% [3a _g (1), 2b _{2u} /Φ _u (1), 2b _{1u} /δ _u (1), 3b _{3u} /π _u (1)]	11 344	0.78
(2) ⁵ B _{1u}	23% [3a _g (1), 2b _{1u} /δ _u (1), 2b _{3u} /Φ _u (1), 3b _{3u} /π _u (1)] 23% [3a _g (1), 2b _{2u} /Φ _u (1), 3b _{2u} /π _u (1), 2b _{1u} /δ _u (1)] 19% [3a _g (1), 1a _u /δ _u (1), 2b _{2u} /Φ _u (1), 3b _{3u} /π _u (1)] 19% [3a _g (1), 1a _u /δ _u (1), 11(1), 2b _{3u} /Φ _u (1)]	11 347	0.78
(2) ³ B _{3g}	35% [1a _u /δ _u (2), 2b _{1u} /δ _u (1), 2b _{3u} /Φ _u (1)] 33% [1a _u /δ _u (1), 3b _{2u} /π _u (1), 2b _{1u} /δ _u (2)]	11 467	0.78
(2) ³ B _{2g}	35% [1a _u /δ _u (2), 2b _{1u} /δ _u (1), 2b _{3u} /Φ _u (1)] 33% [1a _u /δ _u (1), 3b _{2u} /π _u (1), 2b _{1u} /δ _u (2)]	11 467	0.78
(2) ³ B _{1g}	34% [1a _u /δ _u (2), 3b _{2u} /π _u (1), 2b _{3u} /Φ _u (1)] 33% [3b _{2u} /π _u (1), 2b _{1u} /δ _u (2), 2b _{3u} /Φ _u (1)]	12 812	0.78
(1) ³ A _g	51% [1a _u /δ _u (1), 2b _{2u} /Φ _u (1), 2b _{1u} /δ _u ($\bar{1}$), 2b _{3u} /Φ _u (1)]	12 815	0.78

Table S5 – Continued from previous page

State	Character : % [orbital(number of electron)]	ΔE	Ref. weight
(2) ³ B _{1u}	17% [1a _u /δ _u (1), 2b _{2u} /Φ _u ($\bar{1}$), 2b _{1u} /δ _u (1), 2b _{3u} /Φ _u (1)]	13 398	0.77
	20% [3a _g (1), 2b _{2u} /Φ _u ($\bar{1}$), 3b _{2u} /π _u (1), 2b _{1u} /δ _u (1)]		
	20% [3a _g (1), 2b _{1u} /δ _u ($\bar{1}$), 2b _{3u} /Φ _u (1), 3b _{3u} /π _u (1)]		
	15% [3a _g (1), 1a _u /δ _u ($\bar{1}$), 3b _{2u} /π _u (1), 2b _{3u} /Φ _u (1)]		
(2) ³ A _u	15% [3a _g (1), 1a _u /δ _u ($\bar{1}$), 2b _{2u} /Φ _u (1), 3b _{2u} /π _u (1)]	13 402	0.77
	15% [3a _g (1), 1a _u /δ _u ($\bar{1}$), 2b _{3u} /Φ _u (1), 3b _{3u} /π _u (1)]		
	14% [3a _g (1), 3b _{2u} /π _u ($\bar{1}$), 2b _{1u} /δ _u (1), 2b _{3u} /Φ _u (1)]		
	14% [3a _g (1), 2b _{2u} /π _u ($\bar{1}$), 2b _{1u} /δ _u (1), 3b _{3u} /π _u (1)]		
(3) ⁵ B _{3g}	46% [2b _{2u} /Φ _u (1), 3b _{2u} /π _u (1), 2b _{1u} /δ _u (1), 3b _{3u} /π _u (1)]	13 460	0.78
	45% [1a _u /δ _u (1), 3b _{2u} /π _u (1), 2b _{3u} /Φ _u (1), 3b _{3u} /π _u (1)]		
(3) ⁵ B _{2g}	46% [2b _{2u} /Φ _u (1), 3b _{2u} /π _u (1), 2b _{1u} /δ _u (1), 3b _{3u} /π _u (1)]	13 460	0.78
	45% [1a _u /δ _u (1), 3b _{2u} /π _u (1), 2b _{3u} /Φ _u (1), 3b _{3u} /π _u (1)]		
(3) ³ B _{1g}	34% [1a _u /δ _u (1), 2b _{1u} /δ _u (1), 2b _{3u} /Φ _u (2)]	13 638	0.78
	34% [1a _u /δ _u (1), 3b _{2u} /π _u (2), 2b _{1u} /δ _u (1)]		
(2) ³ A _g	47% [1a _u /δ _u (1), 2b _{2u} /Φ _u (1), 2b _{1u} /δ _u (1), 2b _{3u} /Φ _u ($\bar{1}$)]	13 659	0.78
	17% [1a _u /δ _u (1), 2b _{2u} /Φ _u ($\bar{1}$), 2b _{1u} /δ _u (1), 2b _{3u} /Φ _u (1)]		
(2) ⁵ B _{3u}	45% [2a _g /δ _u (1), 1a _u /δ _u (1), 2b _{1u} /δ _u (1), 2b _{3u} /Φ _u 6(1)]	14 688	0.79
	42% [1b _{1g} /δ _u (1), 1a _u /δ _u (1), 2b _{2u} /Φ _u 0(1), 2b _{1u} /δ _u (1)]		
(2) ⁵ B _{2u}	45% [2a _g /δ _u (1), 1a _u /δ _u (1), 2b _{1u} /δ _u (1), 2b _{3u} /Φ _u (1)]	14 688	0.79
	42% [1b _{1g} /δ _u (1), 1a _u /δ _u (1), 2b _{2u} /Φ _u (1), 2b _{1u} /δ _u (1)]		
(2) ³ B _{3u}	30% [3a _g (1), 1a _u /δ _u (1), 2b _{2u} /Φ _u (1), 2b _{1u} /δ _u ($\bar{1}$)]	15 060	0.78
	22% [3a _g (1), 1a _u /δ _u (2), 2b _{3u} /Φ _u (1)]		
	22% [3a _g (1), 2b _{1u} /δ _u (2), 2b _{3u} /Φ _u (1)]		
	11% [3a _g (1), 1a _u /δ _u ($\bar{1}$), 2b _{2u} /Φ _u (1), 2b _{1u} /δ _u (1)]		
(2) ³ B _{2u}	34% [3a _g (1), 1a _u /δ _u (1), 2b _{1u} /δ _u ($\bar{1}$), 2b _{3u} /Φ _u (1)]	15 062	0.78
	22% [3a _g (1), 1a _u /δ _u (2), 2b _{2u} /Φ _u (1)]		
	22% [3a _g (1), 2b _{2u} /Φ _u (1), 2b _{1u} /δ _u (3)]		
	11% [3a _g (1), 1a _u /δ _u ($\bar{1}$), 2b _{1u} /δ _u (1), 2b _{3u} /Φ _u (1)]		
(1) ¹ B _{3u}	32% [3a _g (1), 1a _u /δ _u (1), 2b _{1u} /δ _u (1), 2b _{3u} /Φ _u (1)]	15 336	0.78

Table S5 – Continued from previous page

State	Character : % [orbital(number of electron)]	ΔE	Ref. weight
	21% [3a _g (1), 3b _{2u} /π _u (1), 2b _{1u} /δ _u (2)]		
	21% [3a _g (1), 1a _u /δ _u (2), 3b _{2u} /π _u (1)]		
(1) ¹ B _{2u}	32% [3a _g (1), 1a _u /δ _u (1), 2b _{1u} /δ _u (1), 2b _{3u} /Φ _u (1)]	15 336	0.78
	21% [3a _g (1), 3b _{2u} /π _u (1), 2b _{1u} /δ _u (2)]		
	21% [3a _g (1), 1a _u /δ _u (2), 3b _{2u} /π _u (1)]		
(3) ³ B _{3u}	29% [3a _g (1), 1a _u /δ _u (1), 2b _{2u} /Φ _u ($\bar{1}$), 2b _{1u} /δ _u (1)]	15 370	0.78
	24% [3a _g (1), 2b _{1u} /δ _u (2), 2b _{3u} /Φ _u (1)]		
	23% [3a _g (1), 1a _u /δ _u (2), 2b _{3u} /Φ _u (1)]		
(3) ³ B _{2u}	37% [3a _g (1), 1a _u /δ _u (1), 2b _{1u} /δ _u (1), 2b _{3u} /Φ _u ($\bar{1}$)]	15 382	0.78
	24% [3a _g (1), 2b _{2u} /Φ _u (1), 2b _{1u} /δ _u (3)]		
	23% [3a _g (1), 1a _u /δ _u (2), 2b _{2u} /Φ _u (1)]		
(4) ⁵ A _g	64% [2b _{2u} /Φ _u (1), 3b _{2u} /π _u (1), 2b _{3u} /Φ _u (1), 3b _{3u} /π _u (1)]	15 800	0.78
	20% [2b _{2u} /Φ _u (1), 3b _{2u} /π _u (1), 2b _{1u} /δ _u (1), 2b _{3u} /Φ _u (1)]		
	23% [1a _u /δ _u (1), 3b _{2u} /π _u (1), 2b _{1u} /δ _u (1), 3b _{3u} /π _u (1)]		
	14% [2b _{2u} /Φ _u (2), 2b _{1u} /δ _u (1), 3b _{3u} /π _u (1)]		
	10% [2b _{1u} /δ _u (1), 2b _{3u} /Φ _u (2), 3b _{3u} /π _u (1)]		
(2) ¹ B _{3u}	41% [3a _g (1), 1a _u /δ _u (1), 13(1), 2b _{3u} /Φ _u (1)]	15 850	0.78
	23% [3a _g (1), 2b _{2u} /Φ _u (1), 2b _{1u} /δ _u (2)]		
	23% [3a _g (1), 1a _u /δ _u (2), 2b _{2u} /Φ _u (1)]		
(2) ¹ B _{2u}	41% [3a _g (1), 1a _u /δ _u (1), 2b _{1u} /δ _u (1), 2b _{3u} /Φ _u (1)]	15 850	0.78
	23% [3a _g (1), 2b _{2u} /Φ _u (1), 2b _{1u} /δ _u (2)]		
	23% [3a _g (1), 1a _u /δ _u (2), 2b _{2u} /Φ _u (1)]		
SO-CASPT2 states			
0 _g ⁻	48% (1) ⁵ A _g , 22.45% (1) ³ B _{1g}		0
1 _g	67% (1) ⁵ A _g , 14.59% (1) ³ B _{1g}		2462
1 _u	27% (1) ⁵ B _{2u} , 26.81% (1) ⁵ B _{3u} , 13.24% (1) ⁵ A _u , 12.77% (1) ⁵ B _{1u}		5851
2 _g	85.58% (1) ⁵ A _g		5904
2 _u	24.14% (1) ⁵ A _u , 21.34% (1) ⁵ B _{2u} , 21.31% (1) ⁵ B _{3u}		6266
3 _u	38.85% (1) ⁵ B _{3u} , 24.97% (1) ³ B _{2u}		7197

Table S5 – Continued from previous page

State	Character : % [orbital(number of electron)]	ΔE	Ref. weight
a _g	49.54% (2) ⁵ A _g , 36.86% (1) ⁵ B _{1g}	7240	
b _g	31.53% (3) ⁵ A _g , 23.96% (2) ⁵ B _{1g} , 18.11% (2) ³ B _{3g} , 18.11% (2) ³ B _{2g}	7595	
c _u	22.24% (1) ³ B _{2u} , 21.61% (1) ³ B _{3u} , 12.23% (1) ³ A _u , 10.77% (1) ⁵ B _{2u} , 10.68% (1) ⁵ B _{3u}	7911	
d _g	47.71% (2) ⁵ A _g , 28.33% (1) ⁵ B _{1g} , 15.29% (1) ⁵ B _{2g}	8738	
e _g	32.7% (3) ⁵ A _g , 23.46% (2) ⁵ B _{1g} , 18.02% (1) ⁵ A _g , 12.56% (2) ³ B _{2g} , 12.56% (2) ³ B _{3g}	8971	
f _g	49.36% (1) ⁵ B _{2g} , 49.3% (1) ⁵ B _{3g}	9610	
g _g	72.76% (2) ⁵ A _g	10 193	
h _g	44.58% (3) ⁵ A _g , 22.96% (2) ⁵ B _{1g} , 17.34% (2) ⁵ B _{3g}	10 763	
i _g	63.19% (1) ⁵ B _{1g} , 10.62% (1) ⁵ B _{2g} , 10.62% (1) ⁵ B _{3g}	11 038	
j _u	44.22% (2) ⁵ A _u , 43.57% (2) ⁵ B _{1u}	11 105	
k _u	48.86% (1) ⁵ A _u , 43.03% (1) ⁵ B _{1u}	11 239	
l _u	29.76% (1) ⁵ B _{3u} , 29.64% (1) ⁵ B _{2u}	11 362	
m _u	21.94% (1) ⁵ A _u , 21.78% (1) ⁵ B _{1u} , 18.43% (1) ⁵ B _{3u} , 18.4% (1) ⁵ B _{2u}	11 700	
n _g	19.12% (2) ⁵ B _{2g} , 19.07% (2) ⁵ B _{3g} , 17.44% (1) ³ B _{1g} , 14.82% (1) ¹ A _g	11 817	
o _u	42.88% (1) ³ B _{2u} , 31.88% (1) ⁵ B _{3u}	11 850	
p _g	36.81% (1) ⁵ B _{2g} , 36.81% (1) ⁵ B _{3g} , 9.67% (3) ⁵ A _g	12 253	
q _g	30.81% (1) ⁵ B _{1g} , 23.75% (2) ⁵ A _g , 17.24% (1) ³ B _{2g} , 10.5% (1) ⁵ B _{3g}	12 345	
r _u	36.84% (1) ⁵ B _{1u} , 14.5% (1) ³ B _{3u} , 14.32% (1) ³ B _{2u} , 9.93% (3) ³ A _u	12 539	
s _u	26.69% (2) ³ A _u , 26.67% ³ B _{1u} (2), 21.97% (2) ⁵ A _u , 21.84% (2) ⁵ B _{1u}	12 545	
t _g	53.19% (2) ⁵ B _{1g} , 14.79% (2) ⁵ B _{2g} , 14.79% (2) ⁵ B _{3g}	12 687	
u _u	25.54% (1) ⁵ A _u , 19.8% (1) ³ B _{1u} , 19.02% (1) ⁵ B _{1u}	13 216	
v _u	43.47% (1) ³ A _u , 24.48% (1) ³ B _{1u}	13 241	
w _g	28.83% (2) ⁵ B _{1g} , 20.15% (2) ⁵ B _{2g} , 19.79% (3) ⁵ A _g , 12.91% (2) ⁵ B _{3g} , 12.71% (1) ⁵ B _{2g}	13 394	
x _g	58.26% (1) ⁵ B _{2g}	13 728	
y _g	34.24% (1) ⁵ B _{1g} , 21.57% (1) ³ B _{3g} , 21.56% (1) ³ B _{2g} , 20.21% (2) ⁵ A _g	14 074	
z _g	45.19% (2) ⁵ B _{3g} , 38.99% (2) ⁵ B _{2g}	14 162	
aa _u	47.44% (1) ³ B _{1u} , 14.08% (1) ¹ A _u , 12.08% (1) ⁵ A _u	14 253	
ab _g	32.6% (1) ⁵ B _{3g} , 32.6% (1) ⁵ B _{2g} , 17.93% (2) ³ B _{1g} , 10.46% (2) ⁵ A _g	14 698	
ac _g	35.2% (2) ⁵ B _{3g} , 35.19% (2) ⁵ B _{2g} , 11.61% (2) ³ B _{3g} , 11.61% (2) ³ B _{2g}	14 747	
ad _g	27.69% (1) ⁵ B _{3g} , 27.69% (1) ⁵ B _{2g} , 16.03% (1) ³ A _g , 13.05% (1) ⁵ B _{1g}	14 862	

Table S5 – *Continued from previous page*

State	Character : % [orbital(number of electron)]	ΔE	Ref. weight
ae _u	48.62% (3) ⁵ A _u , 48.07% (3) ⁵ B _{1u}	14 968	
af _g	24.6% (1) ⁵ B _{2g} , 24.55% (1) ⁵ B _{3g} , 14.87% (2) ³ B _{1g} , 12.76% (1) ³ A _g	15 217	
ag _g	57.87% (2) ⁵ B _{3g} , 12.24% (2) ³ B _{2g}	15 786	
ah _u	32.7% (2) ⁵ B _{3u} , 32.65% (2) ⁵ B _{2u} , 15.35% (1) ⁵ B _{3u} , 14.96% (1) ⁵ B _{2u}	15 843	
ai _g	35.75% (3) ⁵ B _{2g} , 35.52% (3) ⁵ B _{3g} , 12.29% (1) ⁵ B _{1g}	15 851	

Table S6: Number of electronic states at MS-CASPT2 level of calculations.

Multiplicity symmetry	Pu		PuO ₂							PuO ₃				PuO ₂ (OH) ₂	
	A _g	A _g	B _{2g}	B _{1g}	B _{3g}	A _u	B _{2u}	B _{1u}	B _{3u}	A ₁	B ₁	B ₂	A ₂	A	B
Singlet	0	2	0	2	0	3	3	3	3	10	9	7	7	7	4
Triplet	27	2	3	3	3	6	7	6	7	16	15	13	14	2	4
Quintet	113	4	3	2	3	4	4	4	4	8	7	6	7	0	0
Septet	103	0	0	0	0	0	0	0	0	0	0	0	0	0	0
Nonet	35	0	0	0	0	0	0	0	0	0	0	0	0	0	0

Table S7: The molecular parameters of PuO₂(g) obtained at the CBS ²DC^M-CCSD(T) level. All electronic states (and their degeneracy in brackets) are not written here, but any levels listed in Table 6 (CBS-²DC^M-EOM-CCSD values) are taken into account in the calculation of thermodynamic functions.

Parameter	Data
Symmetry – sym. number	$D_{\infty h} - 2$
Moment of inertia (g.cm ⁻²)	1.75×10^{-38}
Vibrational frequencies (cm ⁻¹)	170(2), 791, 840
Electronic states (cm ⁻¹)	0(1), 2457(2), 5663(2), 7134(1), 9073(2), 9502(2), etc

Table S8: The molecular parameters of $\text{PuO}_3(\text{g})$. Electronic states are not degenerate, all levels are not written here, but any states listed in Table S3 are taken into account in the calculation of thermodynamic functions.

Parameter	Data
Symmetry – sym. number	$C_{2v} - 2$
Moment of inertia ($\text{g}^3 \cdot \text{cm}^{-6}$)	4.14×10^{-114}
Vibrational frequencies (cm^{-1})	195, 220, 238, 335, 797, 893
Electronic states (cm^{-1})	0, 1235, 1783, 3777, 5660, 6658, 7062, etc

Table S9: The molecular parameters of $\text{PuO}_2(\text{OH})_2(\text{g})$. Electronic states are not degenerate, all levels are not written here, but any states listed in Table S4 are taken into account in the calculation of thermodynamic functions.

Parameter	Data
Symmetry – sym. number	$C_2 - 2$
Moment of inertia ($\text{g}^3 \cdot \text{cm}^{-6}$)	2.044×10^{-113}
Vibrational frequencies (cm^{-1})	103, 185, 225, 240, 270, 386, 415, 491 504, 547, 559, 857, 960, 3855, 3857
Electronic states (cm^{-1})	0, 323, 2222, 3757, 4158, 7268, 7575, etc

Table S10: Standard entropies at 298.15 K (in $\text{JK}^{-1} \text{mol}^{-1}$) with detailed contributions. ^aMoments of inertia have been calculated from geometries got in Ref. S3 within Gaussian09 package. ^bTwo internal rotations have been treated by author with hindered rotor instead harmonic oscillator.

Species	$\text{PuO}_2(\text{g})$		$\text{PuO}_3(\text{g})$			$\text{PuO}_2(\text{OH})_2(\text{g})$	
	this work	Ref. S4	this work	Ref. S4	Ref. S3	this work	Ref. S3
Translational	178.7	178.7	179.4	179.4	179.4	180.2	180.2
Rotational	62.1	62.4	99.8	100.4	97.3 ^a	106.2	105.9 ^a (+35.9 ^b)
Vibrational	22.0	29.2	31.6	33.9	31.6	65.3	48.0
Electronic	0.0	8.5	0.2	5.8	7.7	3.8	7.7
$S_{298\text{K}}^\ominus$	262.9	278.7	311.0	319.4	316.1	355.7	377.8

Table S11: 0 K atomization energies (AE_0 , in kJ mol^{-1}) of PuO_2 , corresponding to the opposite of Reaction R2 at various levels of theory

Method	AE_0
SO-B3LYP	1157.9
SO-UCCSD	1172.6
SO-UCCSD(T)	1255.7
SO-CASPT2	1254.6
SO-CCSD(T) [S7]	1278.6

Table S12: Summary of contributions to the composite calculation of the reaction enthalpies leading to PuO_2 in kJ mol^{-1} , and derived standard enthalpy of formation with its uncertainty. The final average values includes all reactions, except for the ${}^2\text{DC}^{\text{M}}\text{-CCSD}$ and ${}^2\text{DC}^{\text{M}}\text{-CCSD(T)}$ values which are averaged over reactions $\text{R}_3\text{-R}_6$.

Rn.	Method	ΔE_{SF}	ΔZPE	ΔSO	$\Delta_r H^\circ(0\text{ K})$	$\Delta_r H^\circ(298.2\text{ K})$	$\Delta_f H^\circ(298.2\text{ K})$
R_1	SO-B3LYP	-680.0			-640.8	-643.3	-294.3±3.0
	SO-UCCSD	-750.8			-711.6	-714.1	-365.1±3.0
	SO-UCCSD(T)	-795.4	1.8	37.4	-756.2	-758.8	-409.8±3.0
	SO-CASPT2	-737.3			-698.1	-700.6	-351.6±3.0
R_2	SO-B3LYP	-1195.3			-1146.4	-1153.7	-306.2±3.0
	SO-UCCSD	-1210.0			-1161.1	-1168.4	-320.9±3.0
	SO-UCCSD(T)	-1293.1	11.5	37.4	-1244.2	-1251.5	-404.0±3.0
	SO-CASPT2	-1292.0			-1243.1	-1250.4	-402.9±3.0
R_3	SO-B3LYP	-540.0			-534.0	-530.1	-316.6±3.0
	SO-UCCSD	-584.8			-578.8	-574.9	-361.4±3.0
	SO-UCCSD(T)	-630.3		37.4	-624.3	-620.4	-406.9±3.0
	SO-CASPT2	-623.1	-31.4		-617.0	-613.2	-399.6±3.0
	${}^2\text{DC}^{\text{M}}\text{-CCSD}$	-		-	-630.1	-626.2	-412.7±3.0
	${}^2\text{DC}^{\text{M}}\text{-CCSD(T)}$	-		-	-661.2	-657.3	-443.8±3.0
R_4	SO-B3LYP	-291.3			-286.5	-285.3	-297.3±3.0
	SO-UCCSD	-331.4			-326.7	-325.5	-337.5±3.0
	SO-UCCSD(T)	-400.1		37.4	-395.4	-394.2	-406.2±3.0
	SO-CASPT2	-408.7	-32.7		-404.0	-402.8	-414.8±3.0
	${}^2\text{DC}^{\text{M}}\text{-CCSD}$	-		-	-377.0	-375.8	-387.8±3.0
	${}^2\text{DC}^{\text{M}}\text{-CCSD(T)}$	-		-	-430.3	-429.1	-441.1±3.0

Table S12 – *Continued from previous page*

Rn.	Method	ΔE_{SF}	ΔZPE	ΔSO	$\Delta_f H^\circ(0\text{ K})$	$\Delta_f H^\circ(298.2\text{ K})$	$\Delta_f H^\circ(298.2\text{ K})$
R ₅	SO-B3LYP	-202.1			-206.5	-202.9	-337.5±3.0
	SO-UCCSD	-231.4			-235.7	-232.1	-366.8±3.0
	SO-UCCSD(T)	-284.1		37.4	-288.5	-284.8	-419.5±3.0
	SO-CASPT2	-292.7	-41.8		-297.1	-293.4	-428.1±3.0
	² DC ^M -CCSD	-		-	-286.1	-282.5	-417.1±3.0
	² DC ^M -CCSD(T)	-		-	-324.5	-320.8	-455.5±3.0
R ₆	SO-B3LYP	719.5			662.2	648.5	-358.2±3.0
	SO-UCCSD	684.7			627.4	638.5	-368.2±3.0
	SO-UCCSD(T)	632.0		37.4	574.7	585.8	-420.9±3.0
	SO-CASPT2	603.9	-94.7		546.7	557.8	-448.9±3.0
	² DC ^M -CCSD	-		-	576.2	587.3	-419.4±3.0
	² DC ^M -CCSD(T)	-		-	537.8	548.9	-457.7±3.0
Average $\Delta_f H^\circ(298.15\text{ K})$ for PuO ₂							
	SO-B3LYP						-318.4±20.6
	SO-UCCSD						-353.3±16.2
	SO-UCCSD(T)						-411.2±6.6
	SO-CASPT2						-413.7±18.3
	² DC ^M -CCSD						-409.3±14.9
	² DC ^M -CCSD(T)						-449.5±8.8

Table S13: Summary of contributions to the composite calculation of the reaction enthalpies leading to PuO_3 in kJ mol^{-1} , and derived standard enthalpy of formation with its uncertainty. The final average values includes all reactions.

Rn.	Method	ΔE_{SF}	ΔZPE	ΔSO	$\Delta_r H^\ominus(0\text{ K})$	$\Delta_r H^\ominus(298.2\text{ K})$	$\Delta_f H^\ominus(298.2\text{ K})$
R ₁	SO-B3LYP	-781.6			-720.9	-724.8	-375.8±3.0
	SO-CASPT2	-919.7	1.7	59.0	-859.0	-862.8	-513.8±3.0
R ₂	SO-B3LYP	-1554.6			-1479.3	-1490.3	-393.6±3.0
	SO-CASPT2	-1697.7	16.3	59.0	-1622.5	-1633.5	-536.8±3.0
R ₃	SO-B3LYP	-571.7			-560.7	-555.0	-409.2±3.0
	SO-CASPT2	-694.4	-48.0	59.0	-683.4	-677.7	-531.9±3.0
R ₄	SO-B3LYP	-198.5			-189.5	-187.8	-380.3±3.0
	SO-CASPT2	-373.3	-49.9	59.0	-364.3	-362.6	-555.1±3.0
R ₅	SO-B3LYP	-64.8			-69.5	-64.1	-440.6±3.0
	SO-CASPT2	-198.8	-63.7	59.0	-203.5	-198.1	-574.6±3.0
R ₆	SO-B3LYP	1317.6			1233.5	1250.1	-434.4±3.0
	SO-CASPT2	1145.2	-143.0	59.0	1061.2	1077.7	-606.8±3.0
Average $\Delta_f H^\ominus(298.15\text{ K})$ for PuO_3							
	SO-B3LYP						-405.7±22.5
	SO-CASPT2						-553.2±27.5

Table S14: Summary of contributions to the composite calculation of the reaction enthalpies leading to $\text{PuO}_2(\text{OH})_2$ in kJ mol^{-1} , and derived standard enthalpy of formation with its uncertainty. The final average values includes all reactions.

Rn.	Method	ΔE_{SF}	ΔZPE	ΔSO	$\Delta_r H^\ominus(0 \text{ K})$	$\Delta_r H^\ominus(298.2 \text{ K})$	$\Delta_f H^\ominus(298.2 \text{ K})$
R ₁	SO-B3LYP	-1184.2			-1102.6	-1113.6	-764.6±3.0
	SO-CASPT2	-1390.0	34.6	46.9	-1308.5	-1319.4	-970.4±3.0
R ₂	SO-B3LYP	-2675.5			-2548.1	-2572.2	-790.3±3.0
	SO-CASPT2	-2875.8	80.5	46.9	-2748.3	-2772.5	-990.6±3.0
R ₃	SO-B3LYP	-1242.1			-1216.5	-1214.4	-788.1±3.0
	SO-CASPT2	-1420.0	-21.3	46.9	-1394.4	-1392.3	-966.0±3.0
R ₄	SO-B3LYP	-867.5			-828.4	-835.6	-772.6±3.0
	SO-CASPT2	-1109.6	-7.8	46.9	-1070.5	-1077.6	-1014.7±3.0
R ₅	SO-B3LYP	-228.4			-234.0	-232.6	-850.9±3.0
	SO-CASPT2	-428.8	-52.6	46.9	-434.5	-433.0	-1051.4±3.0
R ₆	SO-B3LYP	1154.0			1069.0	1081.6	-844.7±3.0
	SO-CASPT2	916.1	-131.9	46.9	831.1	843.7	-1082.6±3.0
Average $\Delta_f H^\ominus(298.15 \text{ K})$ for $\text{PuO}_2(\text{OH})_2$							
	SO-B3LYP						-801.9±30.3
	SO-CASPT2						-1012.6±38.1

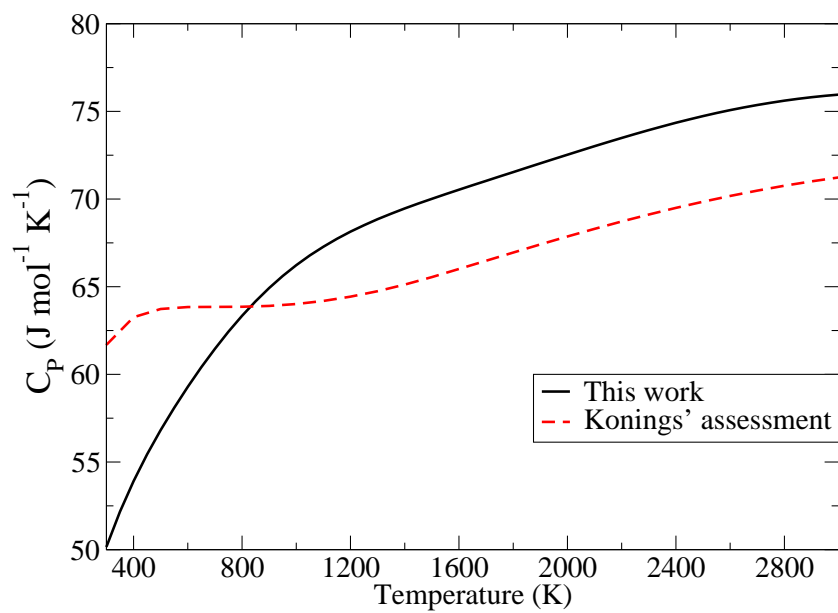


Figure S2: Heat capacity of $\text{PuO}_2(\text{g})$. Konings' assessment refers to Ref. [S4](#)

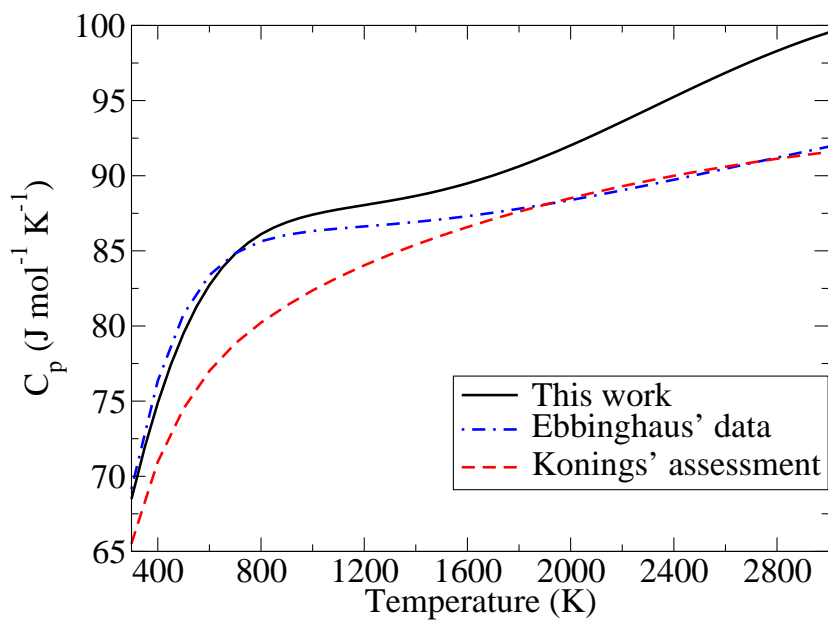


Figure S3: Heat capacity of $\text{PuO}_3(\text{g})$. Konings' assessment refers to Ref. [S4](#) and Ebbinghaus' data to Ref. [S3](#)

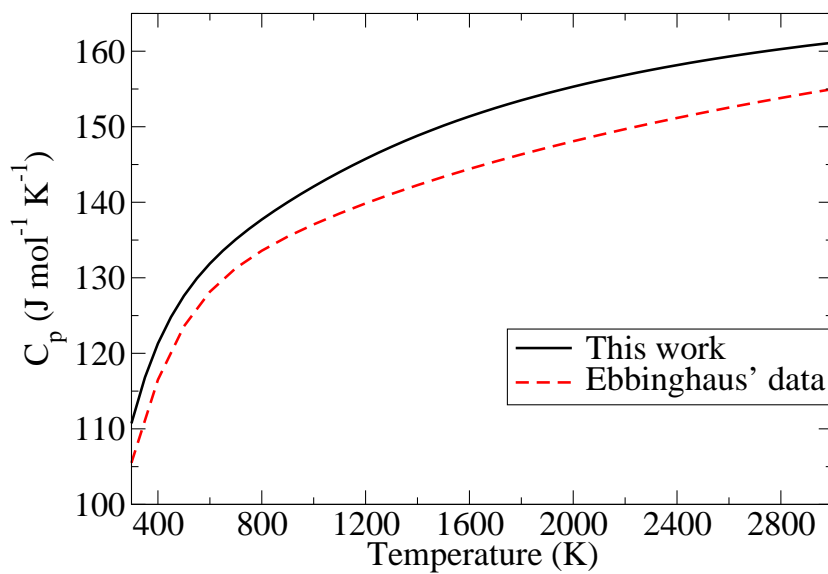


Figure S4: Heat capacity of $\text{PuO}_2(\text{OH})_2(\text{g})$. Ebbinghaus' data refers to Ref. [S3](#)

References

- (S1) Ruscic, B.; Bross, D. H. Active Thermochemical Tables (ATcT) values based on ver. 1.122e of the Thermochemical Network, Argonne National Laboratory (2019); available at ATcT.anl.gov. 2019; <https://atct.anl.gov/>.
- (S2) Lemire, R. J.; Fuger, J.; Nitsche, H.; Potter, P.; Rand, M. H.; Rydberg, J.; Spahiu, K.; Sullivan, J. A.; Ullman, W. J.; Vitorge, P.; Wanner, H. In *Chemical Thermodynamics of Neptunium and Plutonium*; OECD Nuclear Energy Agency, Ed.; Chemical thermodynamics; Elsevier, 2001.
- (S3) Ebbinghaus, B. B. *Calculated thermodynamic functions for gas phase uranium, neptunium, plutonium and americium oxides (AnO_3), oxyhydroxides ($AnO_2(OH)_2$), oxychlorides (AnO_2Cl_2) and oxyfluorides (AnO_2F_2)*; 2002; DOI: 10.2172/15002515.
- (S4) Konings, R. J. M.; Beneš, O.; Kovács, A.; Manara, D.; Sedmidubský, D.; Gorokhov, L.; Iorish, V. S.; Yungman, V.; Shenyavskaya, E.; Osina, E. The Thermodynamic Properties of the f-Elements and their Compounds. Part 2. The Lanthanide and Actinide Oxides. *J. Phys. Chem. Ref. Data* **2014**, *43*, 013101, DOI: 10.1063/1.4825256.
- (S5) Ruscic, B.; Boggs, J. E.; Burcat, A.; Császár, A. G.; Demaison, J.; Janoschek, R.; Martin, J. M. L.; Morton, M. L.; Rossi, M. J.; Stanton, J. F.; et al., IUPAC Critical Evaluation of Thermochemical Properties of Selected Radicals. Part I. *J. Phys. Chem. Ref. Data* **2005**, *34*, 573–656, DOI: 10.1063/1.1724828.
- (S6) Lu, Q.; Peterson, K. A. Correlation consistent basis sets for lanthanides: The atoms La–Lu. *J. Chem. Phys.* **2016**, *145*, 054111, DOI: 10.1063/1.4959280.
- (S7) Feng, R.; Peterson, K. A. Correlation consistent basis sets for actinides. II. The atoms Ac and Np–Lr. *J. Chem. Phys.* **2017**, *147*, 084108, DOI: 10.1063/1.4994725.